Imaginal disc growth factors are *Drosophila* Chitinase-like Proteins with roles in morphogenesis and CO_2 response

Authors

Anne Sustar[1], Liesl Strand[1,2] Sandra Zimmerman[1*], Celeste Berg[1*]

[1]Department of Genome Sciences, University of Washington, Seattle, Washington, [2] Current address: Department of Developmental Biology, Stanford University, Stanford, California

***For correspondence**: caberg@uw.edu; sgzim@uw.edu

Abstract

Chitinase-like proteins (CLPs) are members of the family 18 glycosyl hydrolases, which include chitinases and the enzymatically inactive CLPs. A mutation in the enzyme's catalytic site, conserved in vertebrates and invertebrates, allowed CLPs to evolve independently with functions that do not require chitinase activity. CLPs normally function during inflammatory responses, wound healing, and host defense, but when they persist at excessive levels at sites of chronic inflammation and in tissue-remodeling disorders, they correlate positively with disease progression and poor prognosis. However, little is known about their physiological function. *Drosophila melanogaster* has six CLPS, termed Imaginal disc growth factors (Idgfs), encoded by *Idgf1*, *Idgf2*, *Idgf3*, *Idgf4*, *Idgf5*, and *Idgf6*. In this study we developed tools to facilitate characterization of the physiological roles of the Idgfs by deleting each of the *Idgf* genes using the CRISPR/Cas9 system and assessing loss-of-function phenotypes. Using null lines, we showed that loss-of-function for all six Idgf proteins significantly lowers fertility and viability and compromises germ cell migration. We also showed that Idgfs play roles in epithelial morphogenesis, maintaining proper epithelial architecture and cell shape, regulating E-cadherin and cortical Actin, and protecting these tissues against CO_2 exposure. Defining the normal molecular mechanisms of CLPS is key to understanding how deviations tip the balance from a physiological to a pathological state.

Introduction

Chitinase-like proteins (CLPs) are secreted glycoproteins with properties of cytokines and growth factors (Guan *et al.* 2020; Kawamura *et al.* 1999; Kzhyshkowska *et al.* 2016; Lu *et al.* 2022). Normally, CLPs aid in inflammatory responses, wound healing, and defense against parasites, but they also have a dark side (Di Rosa *et al.* 2016; Mazur *et al.* 2021; Pinteac *et al.* 2021; Sutherland *et al.* 2014). Excess levels of CLPs are associated with diseases exhibiting chronically inflamed tissues, such as cancer, asthma, and arthritis, and there they promote the disease process rather than mitigate it (Di Rosa *et al.* 2016; Kzhyshkowska *et al.* 2016; Lee *et al.* 2011; Mazur *et al.* 2021; Pinteac *et al.* 2021; Qureshi *et al.* 2011).

The enzymatically active members of the family 18 glycosyl hydrolases hydrolyze the glycosidic bonds of chitin, a polysaccharide present in plant, fungal, bacterial, and animal species (Fuhrman *et al.* 1992; Miyashita and Fujii 1993; Samac *et al.* 1990; Tharanathan and Kittur 2003; Watanabe *et al.* 1993). CLPs,

on the other hand, lack hydrolytic activity due to substitution of a key amino acid (glutamic acid) in the protein's catalytic domain (e.g., with glutamine in *Drosophila* Idgfs and human CHI3L2, or with leucine in human CHI3L1) (KIRKPATRICK *et al.* 1995; RECKLIES *et al.* 2002; VARELA *et al.* 2002). This mutation was facilitated by duplication of ancestral chitinases, followed by subsequent mutations and further duplications (BUSSINK et al. 2007). Over evolutionary time, CLPs acquired new functions that do not require chitinase activity.

Extensive research in humans has identified four CLPs: chitinase 3 like 1 (CHI3L1), chitinase 3 like 2 (CHI3L2), oviductal glycoprotein 1 (OVGP1), and stabilin-interacting chitinase-like protein (SI-CLP). Most studies have focused on the expression patterns of CLPs and their clinical relevance as potential biomarkers of disease or as targets for therapy (MAZUR *et al.* 2021; PINTEAC *et al.* 2021). Analyses of the associated molecular mechanisms are limited to a few studies identifying binding partners, receptors, or signaling pathways (ARESHKOV *et al.* 2012; FRANCESCONE *et al.* 2011; FUSETTI *et al.* 2003; GUAN *et al.* 2020; HE *et al.* 2013; KZHYSHKOWSKA *et al.* 2004; KZHYSHKOWSKA *et al.* 2006; LIBREROS *et al.* 2013; LOW *et al.* 2015; MALIK *et al.* 2015; SHAO *et al.* 2009; ZHANG *et al.* 2009), but these studies relied on *in vitro* cell culture, binding assays, immunohistochemistry, or biochemical methods rather than whole-animal models. To understand the molecular mechanisms of CLP function in physiological and pathological contexts, we need to analyze function *in vivo,* preferably in a model organism that would allow definitive functional tests.

The six *Drosophila* Idgfs are encoded by genes located at four sites in the genome: *Idgf1*, *Idgf2*, and *Idgf3* are clustered together on the left arm of chromosome 2 (2L), *Idgf4* lies on the X chromosome, while *Idgf5* and *Idgf6* reside ~ 1.7 Mb apart on the right arm of chromosome 2 (2R) (Figure 1A and Table S1) (KAWAMURA *et al.* 1999; KIRKPATRICK *et al.* 1995; ZUROVCOVA AND AYALA 2002). Although now defined with a common nomenclature, the proteins were originally identified through different routes. Idgf6 (previously called DS47) was isolated from media from cultured Schneider line-2 (S2) cells, which have macrophage-like properties (KIRKPATRICK *et al.* 1995). Idgf1, Idgf2, Idgf3, and Idgf4 were isolated from conditioned media from imaginal disc cell culture (Clone 8 cells) (KAWAMURA *et al.* 1999). Idgf5 was identified by computer search of the *Drosophila* genome (ZUROVCOVA AND AYALA 2002).

Idgf proteins exhibit about 50% amino acid identity with each other and 15–25% amino acid sequence homology to family 18 glycosyl hydrolases, which include the chitinases (KAWAMURA *et al.* 1999; VARELA *et al.* 2002). Consistent with their identification as secreted proteins, Idgfs and their human orthologs have an N-terminal signal sequence and an N-linked glycosylation sequence (ARIAS *et al.* 1994; HU *et al.* 1996; KAWAMURA *et al.* 1999; KIRKPATRICK *et al.* 1995; MENG *et al.* 2010; NYIRKOS AND GOLDS 1990; RENKEMA *et al.* 1998; SCHIMPL *et al.* 2012). The proteins form a characteristic barrel structure composed of eight parallel beta sheets surrounded by eight anti-parallel alpha helices (VARELA *et al.* 2002).

Idgfs promote growth, proliferation, polarization, and motility in cultured cells (KAWAMURA *et al.* 1999). They participate in wound healing, protect against infection by nematodes (BROZ *et al.* 2017; KUCEROVA *et al.* 2016), function in detoxification of cells (BROZ *et al.* 2017), and participate in extracellular matrix organization required for molting (PESCH *et al.* 2016). To accomplish these functions, the Idgfs are not co-regulated, but rather, exhibit distinct expression patterns and respond to different stimuli. In the embryo, *Idgf* RNA is localized in cells adjacent to invaginating cells during tissue morphogenesis (KAWAMURA *et al.* 1999). In larvae and adults, Idgfs are expressed by hemocytes and the fat body (functional equivalent of the liver) and secreted into the hemolymph (CARTON AND NAPPI 2001; IRVING *et*

79 *al.* 2001; KAWAMURA *et al.* 1999; KHUSH AND LEMAITRE 2000; KIRKPATRICK *et al.* 1995; MEISTER *et al.* 2000).
80 Hemocytes and fat body both participate in innate immune responses. In the ovary, Idgfs are expressed
81 in dynamic patterns specific to the different cell types of the egg chamber (ZIMMERMAN *et al.* 2017).
82 Both over- and under-expression in egg chamber cells disrupt epithelial tube morphogenesis (ESPINOZA
83 AND BERG 2020; ZIMMERMAN *et al.* 2017). Thus, Idgfs function in diverse processes in different tissues.

84 In this study, we focused on characterizing the physiological roles of the Idgfs by precisely deleting each
85 of the Idgfs using the CRISPR/Cas9 system and assessing the effects of complete loss of function in
86 various tissues and different life stages. We found that flies lacking all six Idgfs have low viability and
87 fertility. Germ cell migration in these mutants is defective and likely contributes to the observed low
88 fertility. We detected numerous cuticle defects in adults, abnormal epithelial morphogenesis in egg
89 chambers, and segmentation defects in embryos. Finally, we found that Idgfs regulate E-cadherin and
90 cortical Actin and protect epithelia against CO_2 exposure.

91

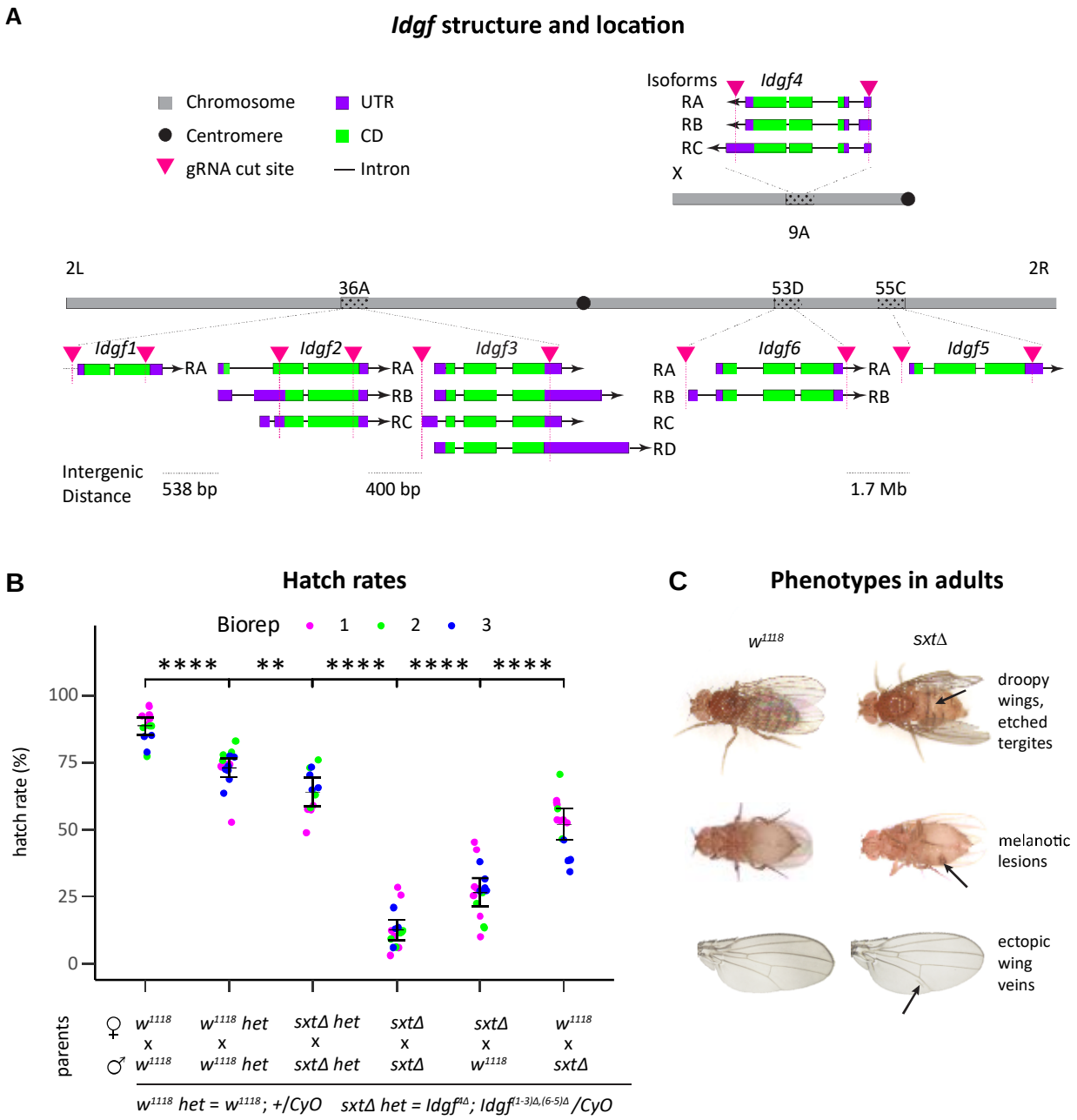

Figure 1 *Idgf* complete knockouts are not entirely lethal. (A) Diagram shows cytological locations of *Idgf* genes and structure of transcript isoforms, including 5' and 3' untranslated regions (purple), coding sequences (green), and introns (thin lines). Black arrows on transcripts indicate the orientation of transcription in the plus (right-pointing) or minus (left-pointing) direction. Arrowheads (magenta) indicate approximate cut sites for deleting each *Idgf* gene. (B) Homozygous and heterozygous *sxtΔ* mutants have low hatch rates relative to control (w^{1118}). Dots represent egg laying assays sampled from three independent biological replicates, ranging from 350-852 eggs analyzed per replicate. Error bars indicate 95% confidence intervals. Significance is based pairwise t-tests with *p*-values adjusted for multiple comparisons (Benjamini-Hochberg), ** denotes $p \leq 0.01$, ****denotes $p \leq 0.0001$. (C) Adult phenotypes. Top row, dorsal view: etched tergites in adult abdomen (arrow). Wings are held out and down ("droopy" wings). Middle row, ventral view: dark cuticle patches (arrow) are reminiscent of melanotic clots. Bottom row: adult wings display ectopic wing veins (arrow). Anterior is up, distal is to the right.

106 # Results

107 ***Idgf* loss of function phenotypes**

108 To begin to understand how Idgfs function, we developed *Idgf* null lines using the CRISPR/Cas9 system.
109 We precisely deleted the coding region of each *Idgf*, creating single, double, triple, and more mutant
110 lines, as well as a line with all six deletions (w^{1118} $Idgf^{4\Delta}$; $Idgf^{(1-3)\Delta,(6-5)\Delta}$, termed "sextuple mutant" and
111 designated from here on as *sxtΔ*) (Figure 1A, Figure S1, and Table S2). In the laboratory environment of
112 rich food and benign growth conditions, we found no highly penetrant defects in any single mutant.
113 *sxtΔ* flies, however, exhibited numerous phenotypes described below.

114 ***sxtΔ mutants have low viability and fertility***

115 Viability and fertility depend on many developmental processes that require patterning, growth, and cell
116 migration. We assessed the function of Idgfs in this context by quantifying hatch rates for offspring from
117 *sxtΔ* homozygous flies and from *sxtΔ* flies carrying the second chromosome CyO balancer (w^{1118} $Idgf^{4\Delta}$;
118 $Idgf^{(1-3)\Delta,(6-5)\Delta}$/*CyO*). We compared these rates to hatch rates of offspring from w^{1118} and w^{1118} carrying
119 the same second-chromosome balancer (w^{1118}; +/*CyO*) (Figure 1B).

120 The expected hatch rate for offspring from w^{1118}; +/*CyO* parents is 75% of all laid eggs (*CyO/CyO* is
121 lethal). In this background, we observed a hatch rate of 73% compared to a hatch rate of 63% in
122 offspring from w^{1118} $Idgf^{4\Delta}$; $Idgf^{(1-3)\Delta,(6-5)\Delta}$/*CyO* parents. The lower hatch rate for embryos in the *sxtΔ*
123 background indicates that reduction of Idgfs moderately impacts embryonic development. For the
124 heterozygous offspring from this cross (embryos carrying the *CyO* chromosome), maternal and zygotic
125 contributions of wild-type Idgfs comes only from the *CyO* chromosome. In the *sxtΔ* homozygous
126 embryos, all zygotic expression of Idgfs is lost. Consistent with maternal loading of *Idgf* transcripts
127 (Zimmerman et al. 2017), maternal and zygotic loss of Idgfs is more detrimental: nearly 90% of eggs laid
128 by *sxtΔ* females mated to *sxtΔ* males fail to hatch. Surprisingly, some escapers survive to adulthood, and
129 when crossed to w^{1118} flies, these escapers are weakly fertile (Figure 1B).

130 Heterozygous offspring from *sxtΔ* females crossed to w^{1118} males have a higher hatch rate (26.5%) than
131 embryos from a cross between *sxtΔ* homozygotes, presumably due to zygotic expression of wild-type
132 Idgfs, and embryos from w^{1118} females crossed to *sxtΔ* males, which have both maternal and potential
133 zygotic *Idgf* expression in embryos, have a 52% hatch rate (Figure 1B). This percentage is lower than the
134 hatch rate from the $Idgf^{4\Delta}$; $Idgf^{(1-3)\Delta,(6-5)\Delta}$/*CyO* cross, possibly reflecting greater fertility of the male
135 carrying the *CyO* balancer, which expresses wild-type Idgfs. These results indicate that both maternal
136 and zygotic expression of wild-type Idgfs participate in embryonic development.

137 To further explore the effect of loss of Idgfs on viability and development, we compared eclosion rates
138 between homozygous (straight-winged) and heterozygous (curly-winged) adult offspring of
139 heterozygous parents (w^{1118}; +/*CyO* or w^{1118} $Idgf^{4\Delta}$; $Idgf^{(1-3)\Delta,(6-5)\Delta}$/*CyO* males and females). Considering
140 the lethality of homozygous *CyO*/*CyO* flies, the expected Mendelian fractions of curly vs. straight-winged
141 adults should be 2/3 heterozygous (curly-winged) and 1/3 homozyous (straight-winged) flies. Chi-
142 squared analysis demonstrates that the relative fractions in the *sxtΔ* background (73% curly, 27%
143 straight) deviates significantly from the relative fractions of wing phenotypes in the w^{1118} background
144 (69% curly, 31% straight) (p = 0.0087) (Figure S2A). Furthermore, *sxtΔ* homozygotes are
145 developmentally delayed compared to w^{1118} homozygotes. The fraction of *sxtΔ* homozygotes eclosing
146 each day relative to the total after 3 days lags behind the w^{1118} homozygotes (Figure S2B).

147 Taken together, these results indicate that loss of all six Idgfs impacts embryonic development, delays
148 embryonic, larval and/or pupal development, reduces overall adult viability, and lowers both male and
149 female fertility.

150 ***Germ cell migration is defective in sxtΔ***

151 In addition to low hatch rates, *sxtΔ* females laid fewer eggs than control females. Consistent with this
152 observation, ovaries from *sxtΔ* adult females were greatly reduced in size compared to control females.
153 Low fertility in *sxtΔ* flies may be the result of defects in germ cell migration and gonad development.
154 Germ cells form at the posterior pole of the embryo and migrate through the gut, guided by attractive
155 and repellent cues, to the somatic gonadal precursors; together these two cell types form the gonads
156 (BEJSOVEC AND MARTINEZ ARIAS 1991; LEBLANC AND LEHMANN 2017). To assess whether low fertility was a
157 consequence of defects in gonad formation, we marked germ cells with anti-Vasa antibody in control
158 (w^{1118}) and *sxtΔ* embryos (Figure S3A, A'). In the mutants, germ cell number is significantly reduced
159 relative to embryos from control flies (Figure S3B, p=0.0002). These defects potentially involve guidance
160 cues, cell adhesion, or polarization. In support of this hypothesis, we have observed a close association
161 of *Idgf6::GFP* transgene expression with germ cells during embryonic Stages 4-7 (Fig S3C).

162 ***Embryos exhibit segmentation defects***

163 The insect body is organized in a series of segments, regulated by segmentation genes consisting of gap,
164 pair-rule, and segment polarity genes. For example, *engrailed* is a segment polarity gene that is
165 expressed in the posterior two rows of each segment (Figure 4A) and participates in the development of
166 denticle belts (GLOVER AND HAMES 1989, pp.65-66). Denticles are hook-like cuticle structures on the
167 ventral side of each larval segment that provide traction for crawling (Figure S4B). During late
168 embryogenesis, the larval epithelial cells that secrete the ventral cuticle have one of two fates: either
169 they remain smooth, or they produce polarized, actin-based protrusions that form the denticles (DILKS
170 AND DINARDO 2010) (Figure S4C). Maintenance of the segmental pattern of alternating smooth and
171 denticle-producing stripes is regulated by the interactions between Engrailed (En), Wingless (Wg), and
172 Patched (Ptc) (GLOVER AND HAMES 1989, pp. 65-66). The pattern of En expression was disrupted in *sxtΔ*
173 mutant embryos, both on a tissue level and within each cell (Figure S4A',B',C',D'). Smooth cuticle
174 overlapped denticle belts, parts of neighboring belts sometimes fused together, single rows of denticles
175 localized within bands of smooth cuticle, and En aberrantly localized to cell membranes (Figure S4D,D')
176 We explored these defects by examining the segmental pattern of denticle-producing and non-denticle-
177 producing cell shapes in late-stage embryos and discovered an array of altered cell shapes and sizes
178 (Figure 4C,C'). This phenotype could be due to patterning defects, or, alternatively, the cells may have
179 achieved proper cell fate but cannot maintain proper positioning within a segment due to loss of cell-
180 junction integrity. Cell polarity may also be affected.

181 ***Adult flies display a variety of cuticle defects and lesions***

182 Adult *sxtΔ* mutant flies display cuticle defects, i.e., etched tergites and "droopy" wings (Figure 1C, top
183 row). Consistent with the role of Idgfs in immune responses (KUCEROVA *et al.* 2016), adults have lesions
184 resembling melanotic clots, which normally occur at the sites of wounds or at sites of pathogen invasion
185 (Figure 1C, middle row, arrow). Adult wings occasionally have ectopic wing veins (Figure 1C, bottom
186 row, arrow), suggesting defects in wing imaginal-disk patterning during larval and early pupal
187 development.

188 **Overall size of *Idgf* mutant adults was not affected**

189 As noted in the Introduction, CLPs have properties of growth factors (ARESHKOV *et al.* 2012; LEE *et al.*
190 2011; SHAO *et al.* 2009). To assess whether loss of Idgfs compromises growth, we quantified fly size by
191 measuring wing area, which correlates well with overall body size (MIRTH AND SHINGLETON 2012; SIOMAVA
192 *et al.* 2016). We compared wing area in four different genotypes and found no significant difference
193 under our culture conditions. Genotypes: w^{1118}, w^{1118} or $Idgf^{(1-3)\Delta}$ in *trans* to a deficiency generated by
194 the Bloomington Stock Center (NIH P40OD018537) (RYDER *et al.* 2004) that uncovers *Idgf*s 1-3 (Table S3),
195 and $Idgf^{(1-3)\Delta}$ in trans to a wild-type chromosome. We found no significant difference between any of
196 these genotypes under our culture conditions. This result implies that these Idgfs do not contribute to
197 growth and proliferation of imaginal discs and histoblast cells during larval and pupal development.
198 Bristle morphology was also normal.

199 ***Dorsal appendage tube formation is disrupted in sxtΔ mutants***

200 Cell migration, polarization, growth, proliferation, and signaling govern the tissue movements and
201 reconfigurations that form morphologic structures such as epithelial tubes. We used our dorsal
202 appendage (DA) tube morphogenesis model to assess the effects of *Idgf* loss of function during
203 oogenesis (Figure 2A). DA tubes produce eggshell structures that facilitate gas exchange for the
204 developing embryo, and they are made by a subset of follicle cells in late-stage egg chambers. The egg
205 chamber consists of 15 germline-derived nurse cells, one oocyte, and a surrounding monolayer of
206 somatic epithelial cells consisting posteriorly of columnar cells and anteriorly of squamous cells (termed
207 "stretch" cells). The tubes develop from two patches of precursor cells in the follicular epithelium and,
208 through cell intercalation and cell shape change, elongate by migrating anteriorly over the stretch cells
209 and beneath the extracellular matrix (DORMAN *et al.* 2004; OSTERFIELD *et al.* 2013; RITTENHOUSE AND BERG
210 1995; WARD AND BERG 2005). The tube cells secrete eggshell protein into the tube lumen, providing a
211 readout for tube formation, similar to the way a mold forms a sculpture (DAs) (Figure 2A, right image).
212 This highly conserved process of tube formation is a wrapping mechanism akin to mammalian neural
213 tube formation (OSTERFIELD *et al.* 2017).

214 We previously observed disruption of DA morphogenesis using *Idgf1* and *Idgf3* overexpression (ESPINOZA
215 AND BERG 2020; ZIMMERMAN *et al.* 2017) and *Idgf* RNAi for each single mutant (ZIMMERMAN *et al.* 2017).
216 Since null mutations are the gold standard in genetics, we asked "What about complete knockout of
217 *Idgfs*?" We compared the DA phenotypes of eggs laid by each single *Idgf* CRISPR-null mutant and the
218 *sxtΔ* mutant to the DAs of eggs laid by control (w^{1118}) flies and categorized the phenotypes as mild,
219 moderate, or severe by scoring the DAs while blinded to the genotypes (Figure 2B). To limit the
220 influence of potential background mutations, we assessed the phenotypes produced by single mutant
221 genotypes *Idgf1Δ* through *Idgf6Δ* by placing each *Idgf* deletion chromosome *in trans* to a deficiency
222 chromosome generated independently by the Bloomington Stock Center (NIH P40OD018537) (RYDER *et*
223 *al.* 2004). Note that none of the deficiencies produced DA phenotypes on their own (Table S3). The *sxtΔ*
224 mutant was assessed homozygously due to the unfeasibility of creating flies heterozygous with
225 deficiencies spanning each of the six deleted *Idgf* loci.

226 Approximately 50% of eggs laid by the *sxtΔ* mutants and 18% of the *Idgf6*Δ mutants had moderate or
227 severe phenotypes, but both of these percentages varied somewhat from experiment to experiment
228 (see below). The other single mutants (*Idgf1*Δ, *Idgf2*Δ, *Idgf3*Δ, *Idgf4*Δ, and *Idgf5*Δ) did not exhibit

229 significant levels of defects [Figure 2C (i)]. Expression of an *Idgf6::GFP* transgene in a *sxtΔ* mutant
230 background partially rescued the *sxtΔ* DA phenotype [Figure 2C (ii)].

231 Overall, these results provide evidence for important physiologic roles of Idgfs in tissue morphogenesis,
232 potentially including cell polarization, migration, adhesion, and signaling.

233

234

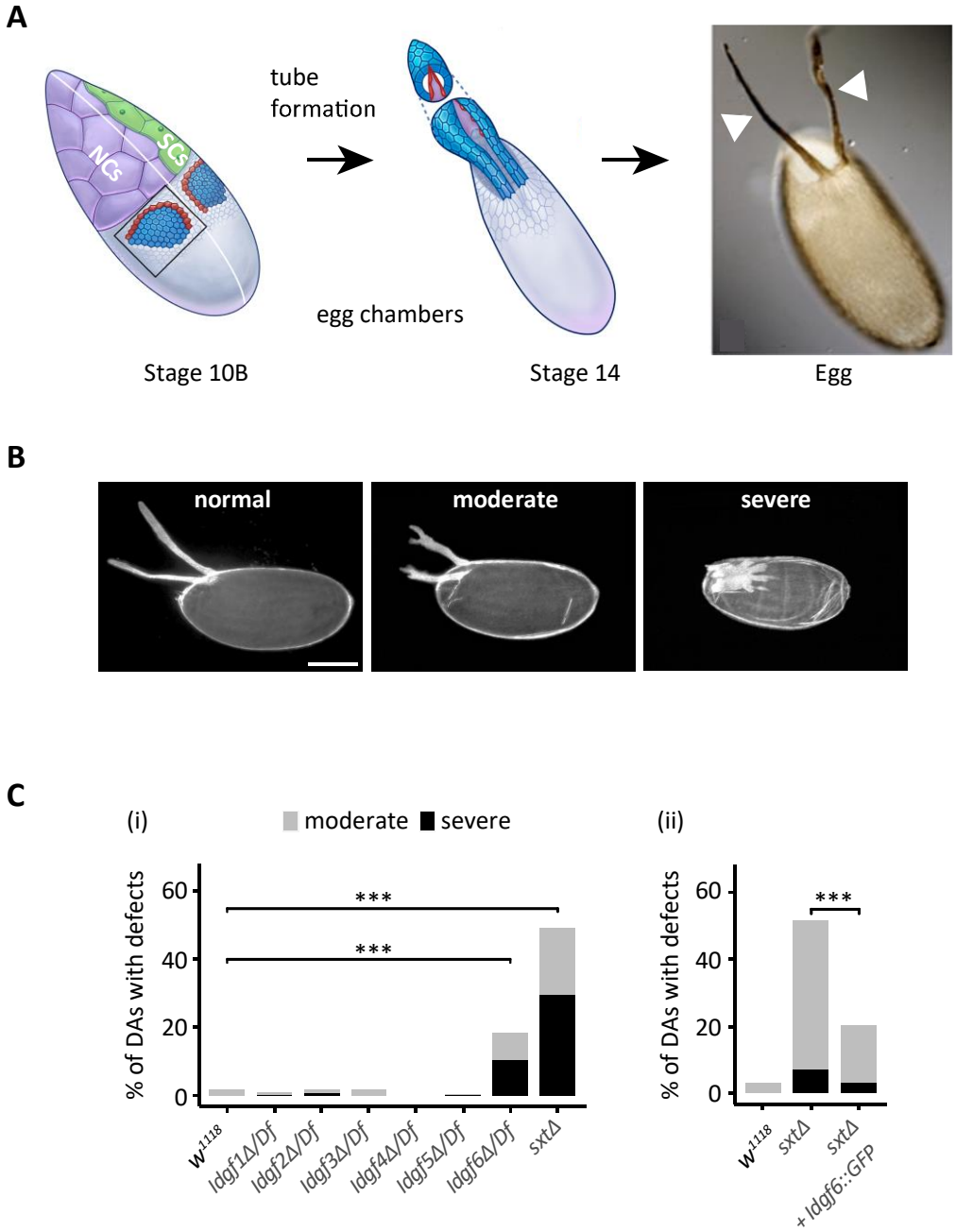

235

236 **Figure 2 Dorsal appendage tube formation and defects in *Idgf* mutants.** (A) Dorsal appendage formation. Roof
237 cells (blue) and floor cells (red) change shape and reorganize to make two DA tubes. Stretch cells (green), cut away
238 to show nurse cells (purple), guide tube elongation. Dorsal appendages (arrowheads) of the laid egg bring air to
239 the embryo that is developing inside the eggshell. (B) Representative examples of DA morphology categorized into
240 normal, moderate, and severe phenotypes. Scale bar = 100µm. (C) Moderate and severe DA phenotypes are
241 significantly increased in eggs laid by *Idgf6*Δ/*Df* and *sxtΔ* females indicating defects in tubulogenesis during
242 oogenesis. *Idgf1*Δ/*Df*, *Idgf2*Δ/*Df*, *Idgf3*Δ/*Df*, *Idgf4*Δ/*Df,* and *Idgf5*Δ/*Df* single mutants do not significantly affect DA
243 morphology [C(i)]. Expression of a wild-type *Idgf6* transgene in *sxtΔ* mutant females partially rescues DA

244 morphology [C(ii)]. Deficiency chromosomes specific to each mutant are listed in Table S3. *** indicates $p<0.001$,
245 X^2 test for trends in binomial proportions (ROSNER 2000).
246

Idgfs protect against effects of CO_2 exposure

While analyzing the DA defects in eggs laid by *Idgf* mutants, we observed variability in penetrance and expressivity. Initially, we found differences in the percentage and severity of DA defects for eggs laid by *Idgf6Δ* females. Because these two sets of experiments (*Idgf6Δ* vs. other single *Idgf* mutants) were performed by two different lab workers, we asked whether these differences were biological or whether the variability was due to a difference in technique between lab workers (e.g., age of flies, overcrowding, or CO_2 exposure). Intriguingly, we determined that there was variability in whether flies were exposed to CO_2 when they were transferred to fresh egg-laying plates. This observation raised the question as to whether loss of *Idgf* function rendered flies more sensitive to CO_2.

To compare CO_2 sensitivity between wild-type and mutant flies, we assessed DA morphology on eggs laid by w^{1118} flies and *Idgf* mutants by using several different regimes of CO_2 exposure. Treating adult females to 100% CO_2 for 60 seconds twice per day (~every 12 hours) for 3.5 days (Figure S5A) resulted in a significant increase in DA defects on the eggs laid by *Idgf6Δ* and *sxtΔ* mutants, but not on the w^{1118} eggs nor in any of the other single mutants (*Idgf1Δ* through *Idgf5Δ*).

Since tissue and cellular responses to carbon dioxide depend on the length and severity of exposure (HELENIUS *et al.* 2016; HELENIUS *et al.* 2009; SHARABI *et al.* 2009a; SHARABI *et al.* 2009b), we asked if a prolonged exposure to a lower level of CO_2 would have a similar effect. We exposed *sxtΔ* mutant and w^{1118} adult flies to either 20% CO_2 or 100% air and evaluated DA morphology at 1.5 – 2 days and 7-8 days of exposure. Exposure to CO_2 over either of these time periods did not significantly increase DA defects in eggs laid by *sxtΔ* mutants (Figure S5B).

We next asked whether the effect of CO_2 exposure was directly due to the CO_2 itself or due to hypoxia, the transient absence of oxygen. To distinguish between these two hypotheses, we exposed flies to 100% N_2 for five minutes followed by DA analysis at 8 – 10 hours and 2 days after exposure. We did not observe a significant effect on DA morphology following this treatment, indicating that the increase in DA morphology defects was directly due to CO_2 exposure rather than hypoxia (Figure 3A).

These results suggest that Idgf proteins protect tissues against acute CO_2 exposure. If this hypothesis is correct, expression of Idgf protein should rescue the DA mutant phenotype associated with high CO_2. To test this prediction, we used a GFP-tagged transgene, *Idgf6::GFP*, in which Idgf6 is fused in-frame at its C-terminus to superfolder GFP (SAROV *et al.* 2016). We expressed this transgene in the *Idgf6Δ* and *sxtΔ* mutants and compared the DA phenotypes to the same mutants lacking the transgene. We exposed the flies to a single pulse of 100% CO_2 for one minute and analyzed DA defects at 8 – 10 hours and 2 days after exposure (Figure 3B). While both mutants exhibited defects at 8 – 10 hours after exposure, *Idgf6Δ::GFP* expression restored the percentage of DA defects to pre-exposure levels in the *Idgf6Δ* mutants, and it reduced the DA defects in the *sxtΔ* mutants but not to the level of statistical significance. After 2 days, the DA defects in both mutants recovered to pre-exposure levels. These results demonstrate that this gene—environment interaction is due to the loss of Idgfs. Significantly, expression of a single Idgf protein can rescue or ameliorate the DA phenotype in *Idgf* mutants.

To examine the time course following acute CO_2 exposure on a finer scale, we exposed adult *sxtΔ* flies to a single pulse of 100% CO_2 for one minute, followed by hourly DA defect analysis (Figure 3C). Defects peaked at 6 – 10 hours after exposure and then recovered by ~27 hours after exposure.

287 In addition to the developmental roles for Idgfs in normoxia, these results support a hypothesis that
288 Idgfs protect against morphogenetic disruption following acute CO_2 exposure.

289

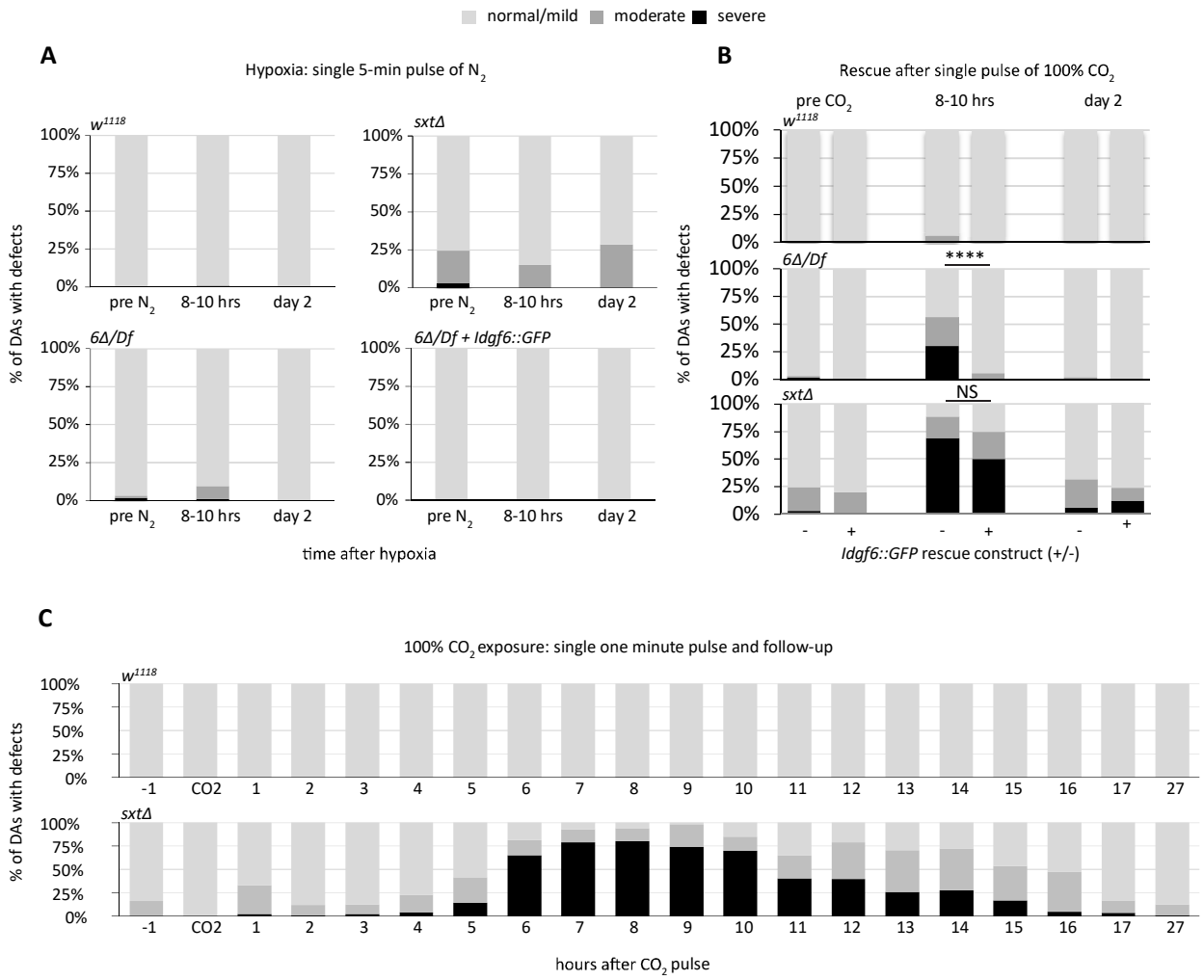

Figure 3 Idgfs protect against CO_2 exposure. (A) Effect of hypoxia on DA phenotype. Air is replaced with 100% N_2 for 5 min to induce hypoxia. DA phenotype is not significantly affected by hypoxia. (B) Expressing a single copy of a wild-type *Idgf6* transgene rescues the DA *Idgf6Δ* phenotype induced by a single, 1-min pulse of 100% CO_2. The sxtΔ phenotype is partially but not significantly rescued (p=0.32). Proportions of defects peak at 8-10 hours after the CO_2 pulse. The *Idgf6Δ* deletion is transheterozygous with a deficiency chromosome to cover potential background mutations. **** denotes significance ($p \leq 0.0001$, X^2 test), NS=not significant. (C) Hourly assessment of DA phenotype following a 1-minute pulse of 100% CO_2. DA defects in eggs laid by *sxtΔ* females peak at 7-10 hours after CO_2 exposure.

300 ***Actin but not E-cadherin is disrupted in egg chambers after CO_2 exposure***

301 How do Idgfs function in DA morphogenesis, and how does acute exposure to CO_2 impact that process?
302 One hypothesis is that Idgfs are necessary for patterning the DA primordial cells. A second hypothesis is
303 that Idgfs regulate cell morphology and epithelial tissue dynamics. To test these hypotheses, we
304 exposed adult females to 100% CO_2 for one minute and then waited for 20-30 minutes before
305 dissecting, fixing, and staining the ovaries. We then examined patterning and cell morphology of the DA-
306 forming cells using antibodies against Broad, a transcription factor that specifies the DA roof-forming
307 cells, and against E-cadherin, an adhesion protein that outlines cell shapes (Dorman et al. 2004; Ward
308 and Berg 2005; Ward et al. 2006).

309 Patterning was normal in both w^{1118} and *sxtΔ* in both the exposed and unexposed egg chambers as
310 revealed by two patches of ~ 50, high-Broad-expressing cells residing just lateral to the dorsal midline
311 (Figure 4A-C). Cell morphology in the DA patches, however, was more disorganized, and E-cadherin was
312 disrupted in the *sxtΔ* exposed egg chambers relative to the exposed w^{1118} and unexposed *sxtΔ* egg
313 chambers (Figure 4A'-C', rectangles). DA cell circumferences were abnormally large in both the exposed
314 and unexposed *sxtΔ* mutants relative to the DA cells in the exposed w^{1118} egg chambers (Figure 4A'-C',
315 rectangles, and Figure 4D-E, rectangles). After exposure to CO_2, *sxtΔ* DA-forming cells were further
316 disrupted by a dramatic loss of Actin from both the cell junctions and the basal surfaces (Figure 4G). In
317 contrast, cell shapes and Actin levels looked normal in the w^{1118} DA-forming cells (Figure 4F).

318

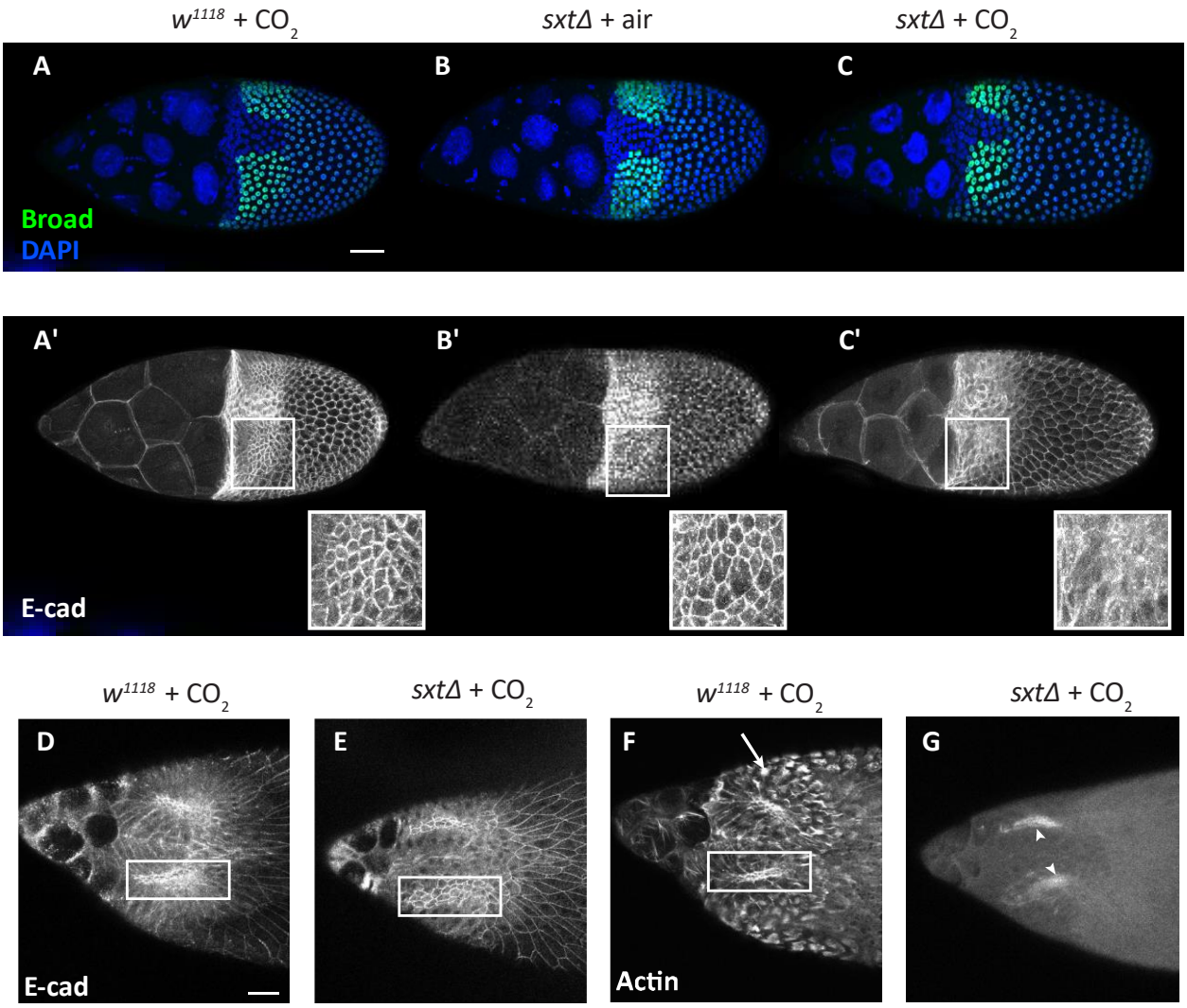

Figure 4 Patterning and cell morphology in DA-forming cells. (A-C') Stage 10B egg chambers. Top row (A-C): Broad (green) marks the roof cells in the DA primordium, DAPI (blue) indicates the nuclei. Patterning is normal in *sxtΔ* mutant exposed to CO_2. Lower row (A'-C'): E-cadherin delineates the apico-lateral cell junctions in follicle cells. Cell morphology is abnormal in *sxtΔ* mutant DAs, and E-cadherin localization is disrupted after a single pulse of 100% CO_2 exposure (white rectangles indicate DA-forming cells). (D-G) Stage 12 egg chambers. DA roof cells (white rectangles) are abnormally large in the *sxtΔ* mutant (E) compared to control (w^{1118}) (D) egg chambers. (F) As shown in w^{1118} egg chambers, basal cell membranes normally exhibit bright spots of Actin localization (arrow). (G) In *sxtΔ* mutants, Actin is lost from cell membranes after CO_2 exposure. Arrowheads in the *sxtΔ* + CO_2 image indicate chorion autofluorescence.

330 We quantified E-cadherin and Actin in the DA-forming follicle cells by measuring fluorescent intensities
331 across cell membranes using ImageJ (Figure 5, Figure S6) and calculating the total area under the plot
332 profiles. To assess whether potential differences in intensity might be stage or cell-type specific, we
333 analyzed roof cells, floor cells, and main-body follicle cells at Stage 10B, just prior to tube wrapping, and
334 at Stage 12, during tube elongation (Figure 5A and Figure S6A). E-cadherin intensity was lower in *sxtΔ*
335 mutants relative to w^{1118} control flies ($p \leq 0.05$), but it was not significantly affected by CO_2 exposure
336 (Figure 5B,C and Figure S6B). In contrast, Actin levels were similar in w^{1118} and *sxtΔ* mutants but
337 dropped quickly in both samples upon exposure to CO_2 ($p \leq 0.05$) (Figure 5B',C' and , Figure S6B'). After
338 30 minutes, Actin intensity recovered in the control egg chambers but remained low in the *sxtΔ* mutant
339 samples (Figure 4F,G). These results suggest that Idgfs regulate E-cadherin expression or stability in
340 normoxia and that they impact Actin dynamics in response to CO_2.

341

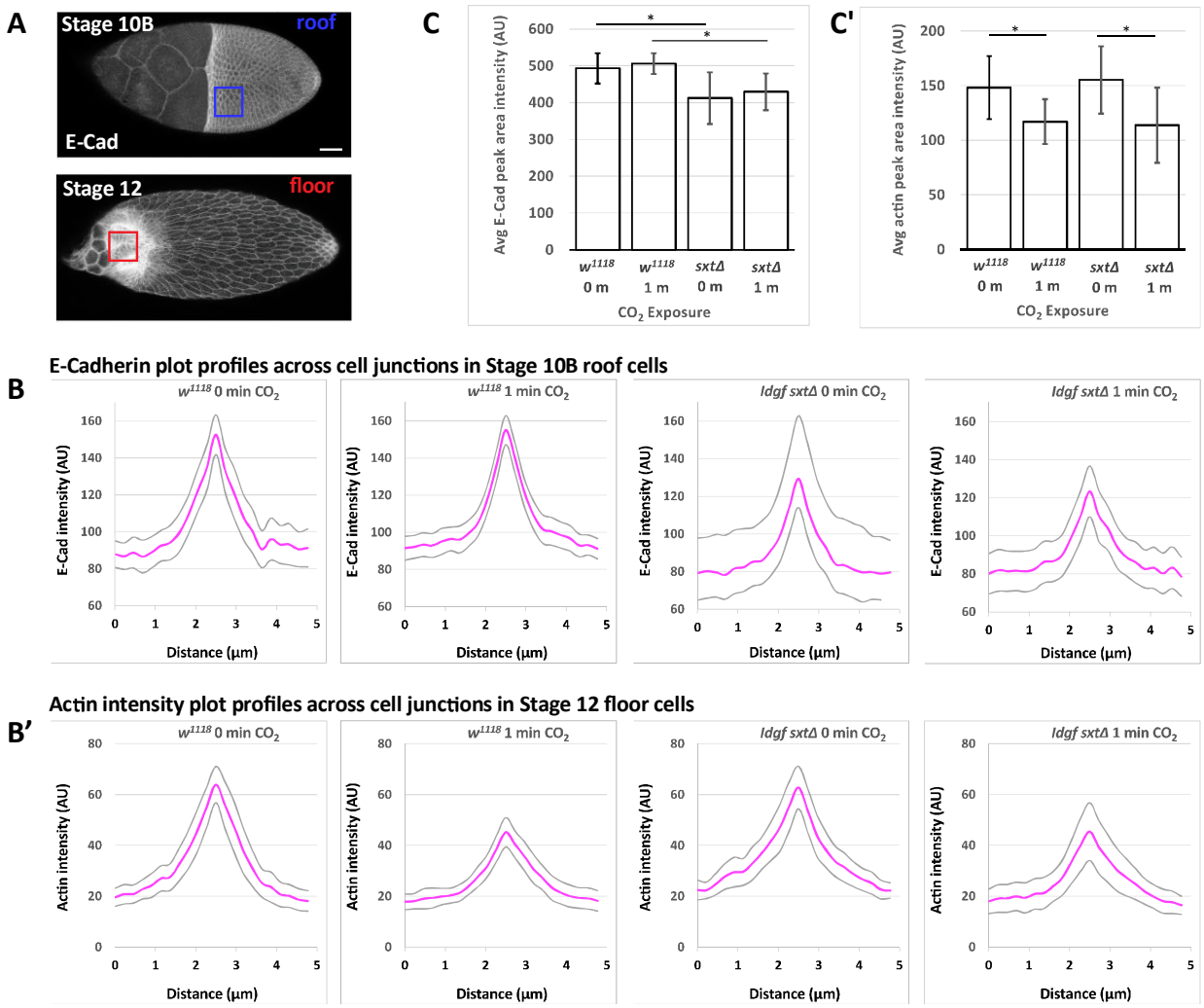

Figure 5 Quantification of cortical Actin and E-Cadherin intensity in DA cells. (A) E-Cadherin and Actin in Stage 10B roof cells (blue square) and Stage 12 floor cells (red square). Scale bar = 50 µm. (B) Comparison of w^{1118} and *sxtΔ* fluorescence intensity plot profiles averaged across three cell membranes, from the center of one cell to the center of the neighboring cell, averaged over at least 6 egg chambers for each genotype and each exposure regime as indicated. Plots show mean (magenta) and confidence limits (gray). (C) Integrated area under the curves in B and B' averaged over all measurements. Error bars show 95% confidence limits. * denotes $p \leq 0.05$, Student's *t*-test, Benjamini-Hochberg adjusted *p*-values.

351 ***Actin is disrupted in Stage 8-12 embryos after CO_2 exposure***

352 To ask whether Idgfs regulate E-cadherin and Actin in other contexts, we examined E-cadherin and Actin
353 during embryonic development. We exposed w^{1118} and *sxtΔ* embryos of all stages to 100% CO_2 or
354 pressurized air for 2 minutes before de-chorionating, fixing, and staining. Since embryos comprise
355 numerous distinct cell types, we focused on cells near the surface that were relatively uniform in size
356 and easy to measure. We chose ectodermal cells located between the mid-lateral cells and lateral edge
357 of the germ band in abdominal segments 2-6 and measured these cells during the extended germ band
358 stages (late Stage 8 – early Stage 12). Under these conditions, we observed no significant difference
359 between E-cadherin levels in w^{1118} embryos or *sxtΔ* mutant embryos under any of the three conditions
360 (Figure 6A, Figure 6A'). Actin levels also did not differ significantly in w^{1118} embryos between any of the
361 three treatments (Figure 6B, Figure 6B'). However, Actin levels were significantly lower in *sxtΔ* mutants
362 exposed to CO_2 compared to unexposed embryos or embryos exposed to air in either genotype. Taken
363 together, these results support our hypothesis that CO_2 exposure disrupts Actin in embryonic epithelia.

364

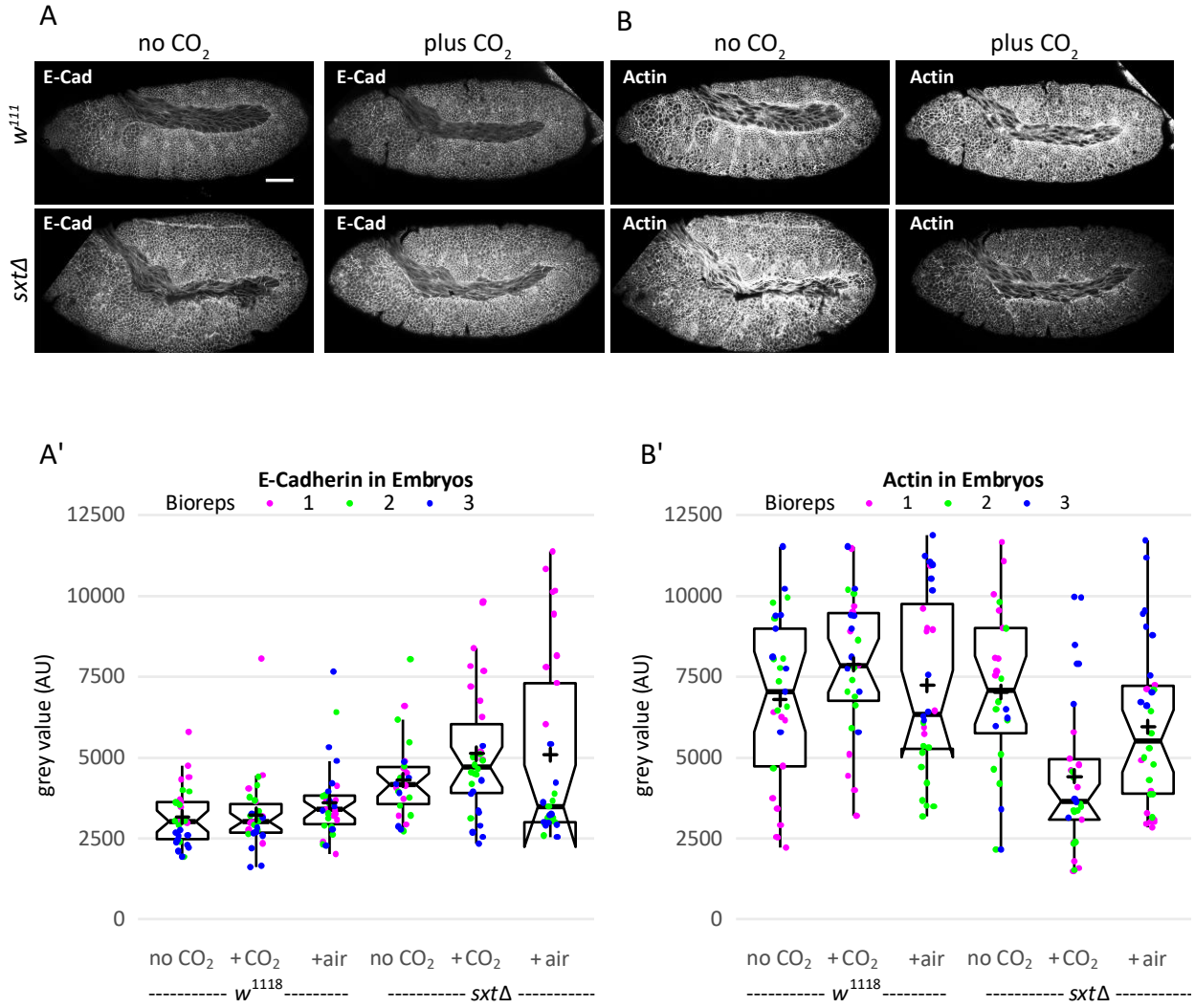

Figure 6 Quantification of cortical Actin and E-Cadherin intensity in Stage 8-12 embryos. (A, B) Representative embryo images showing E-cadherin (A) and Actin (Rhodamine phalloidin) (B) comparing genotypes and CO_2 regime as indicated. Scale bar = 50 µm. (A', B') Comparison of *w*^{1118} and *sxtΔ* fluorescence intensity measured across 6 cell membranes per embryo, from the center of one cell to the center of the neighboring cell. The colors represent different biological replicates. Each point in the graphs represents the average of the areas under the 6 plot profiles per embryo. The notches on the box plots represent the 95% confidence interval of the medians (horizontal lines), ±1.57*IQR/sqrt(n). IQR = interquartile range. + signs = means. Notches that double back occur when the uncertainty of the median exceeds the IQR. Non-overlapping notches are strong evidence that their medians significantly differ.

378 When analyzing Actin dynamics in egg chambers, we noticed that some cell types were more sensitive
379 to CO_2 exposure than others and that the effect of CO_2 exposure on Actin perdured over a longer period
380 in *sxtΔ* mutants compared to w^{1118} controls. We therefore asked whether we might see more dramatic
381 effects in embryos if we exposed embryos during cellularization, a period when Actin function is crucial
382 (SOKAC *et al.* 2022). We also reasoned that embryonic cells might be protected from CO_2 exposure by
383 the eggshell. We therefore exposed early-stage embryos to 100% CO_2 and increased the exposure time
384 to six minutes. Embryos were allowed to age for 30 minutes before fixing them and staining with
385 phalloidin. We measured Actin fluorescence intensity across cell membranes in syncytial blastoderm
386 embryos during stages 3-5. Prior to cellularization in Stage 5, nuclei in the syncytial blastoderm embryo
387 are surrounded by Actin extensions (called pseudofurrows) at the periphery. In Stage 5, the Actin
388 furrows extend around the nuclei to form a single layer of cells surrounding the yolky core. At these
389 stages, the cells are uniform in size and shape, facilitating uniformity in measurements. As we observed
390 in egg chambers, loss of Actin was significant in early embryos after exposure to CO_2 but did not differ
391 significantly between w^{1118} and *sxtΔ* (Figure 7A,B,C).

392

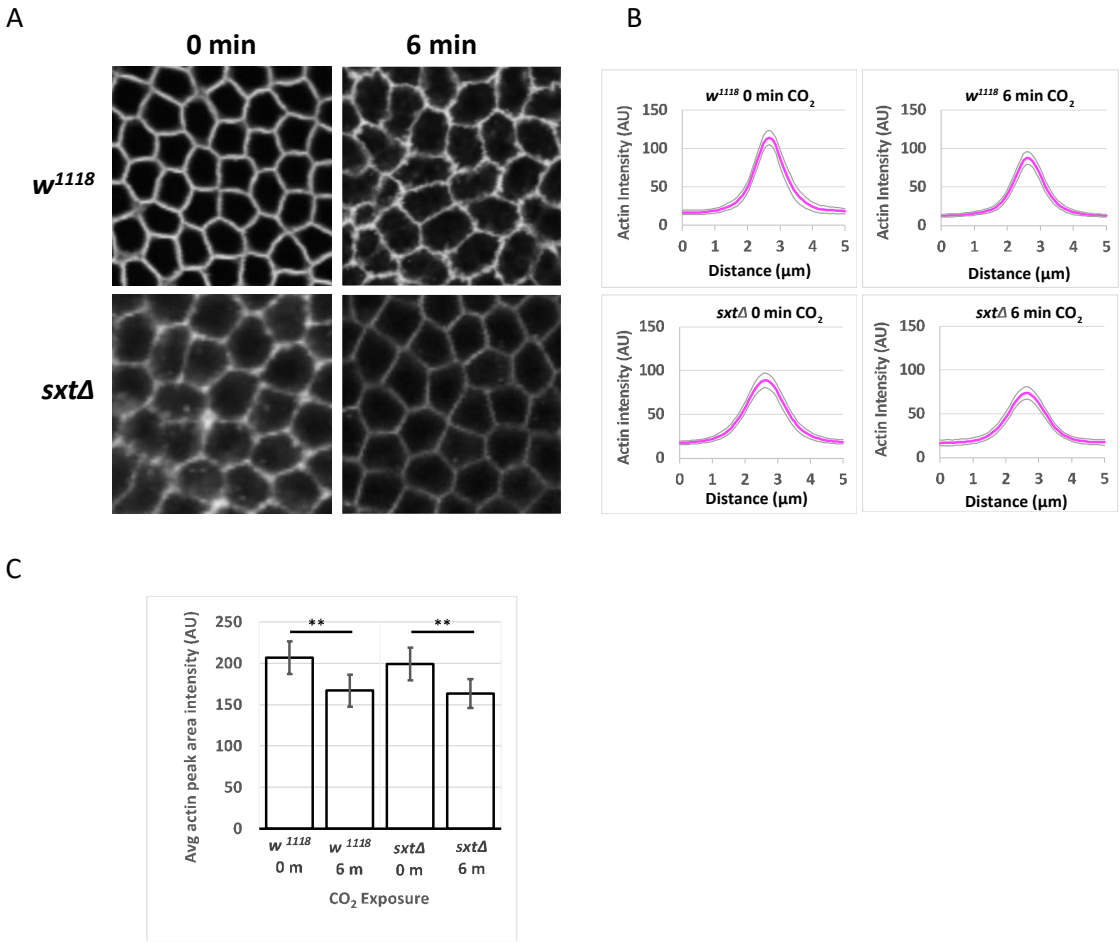

Figure 7 Quantification of cortical Actin intensity in Stage 3-5 embryos. (A) Actin in early embryos comparing genotypes and CO_2 regime as indicated. (B) Comparison of *w*^{1118} and *sxtΔ* fluorescence intensity plot profiles averaged across 6 cell membranes, from the center of one cell to the center of the neighboring cell, averaged over at least 10 Stage 3-5 embryos for each genotype and each exposure regime as indicated. Plots show mean (magenta) and confidence limits (gray). (C) Integrated area under the curves in B averaged over all measurements. Error bars show 95% confidence limits. ** denotes $p \leq 0.01$, Student's *t*-test, Benjamini-Hochberg adjusted *p*-values.

401 # Discussion

402 We investigated the *in vivo* roles of *Drosophila* Imaginal disc growth factors throughout development.
403 Previous studies have sought to characterize the function of individual Idgfs using RNAi or in cell culture.
404 We are the first to delete each of the Idgfs and develop fly lines with single or multiple deletions of the
405 Idgfs, including flies null for all six Idgfs. Using these tools, we found that loss of all Idgf function results
406 in a variety of phenotypes.

407 In *Idgf sxt*Δ mutants, gonads form with significantly reduced germ cell numbers. Most germ cells are
408 lost or die before they reach the somatic gonadal precursor cells, consistent with the low fertility we
409 observed in *sxt*Δ adults. Normally, germ cells form at the anterior pole of the embryo and are taken into
410 the midgut primordium during gastrulation. They initially form a tight cluster in the midgut, but
411 subsequently extend protrusions toward the midgut cells, lose adhesion from each other, disperse,
412 migrate individually through the midgut, and associate with somatic gonadal precursors cells to form the
413 gonads (Review: RICHARDSON AND LEHMANN 2010). To migrate, germ cells become polarized and extend
414 protrusions toward the midgut cells. One hypothesis is that Idgfs participate in remodeling of cell
415 junctions and Actin dynamics in migrating cells, consistent with our finding that loss of all Idgfs disrupts
416 E-cadherin and Actin in certain contexts. A second hypothesis is that loss of Idgf function disrupts
417 polarization and protrusiveness of primordial germ cells, consistent with a previous study demonstrating
418 that Idgfs promote cell motility and protrusiveness in cell culture (KAWAMURA *et al.* 1999). Initial
419 polarization of germ cells requires the G-protein-coupled receptor (GPCR) Trapped in endoderm 1
420 (Tre1), which is expressed in the germ cells and coincides with a redistribution of the Gβ subunit and
421 adherens junction proteins such as Rho1 and E-cadherin (KUNWAR *et al.* 2008). Tre1 is also important for
422 migration across the midgut by signaling through small G proteins and the GTPase Rho1 (KUNWAR *et al.*
423 2003). Studies have identified other key regulators of germ cell migration, such as the lipid phosphate
424 phosphatases, Wunen and Wunen-2 (HANYU-NAKAMURA *et al.* 2004), the small acidic protein, 14-3-3ε
425 (TSIGKARI *et al.* 2012), and pathways such as JAK/STAT (BROWN *et al.* 2006; LI *et al.* 2003). CLPs are known
426 to have properties of cytokines (LEE *et al.* 2011), raising the question of whether Idgfs may promote
427 guidance cues for migrating germ cells. We have observed that Idgf6 associates with migrating germ
428 cells from embryonic Stages 4-7; this association is lost by Stage 10. How Idgfs might interact with these
429 components or otherwise participate in germ cell migration will require further study.

430 Consistent with studies showing expression of Idgfs throughout development, we showed that hatch
431 rates are severely reduced in *sxtΔ* homozygous embryos from *sxtΔ* parents. This effect of loss of all
432 maternal and zygotic Idgfs was ameliorated by adding either maternal, zygotic, or both maternal and
433 zygotically expressed Idgfs. Interestingly, offspring of parents where both parents carry a *CyO*
434 chromosome in a *sxtΔ* background have a higher hatch rate than offspring of w^{1118} females crossed to
435 *sxtΔ* males, even though both scenarios produce embryos that presumably receive both maternal and
436 zygotically expressed Idgfs. Perhaps *sxtΔ* males are less fertile than their *sxtΔ* counterparts carrying the
437 *CyO* chromosome, which expresses wild-type Idgfs. One hypothesis is that the sxtΔ male's fertility is
438 compromised by defective germ cell migration, consistent with our finding that germ cell migration is
439 defective in *sxtΔ* embryos.

440 Further, we found that the proportions of homozygous vs. heterozygous offspring produced by
441 heterozygous parents deviate significantly from the expected Mendelian ratios, reflecting greater
442 lethality of the homozygotes from embryonic through adult stages. Our observation that eclosion is

443 delayed in *sxtΔ* mutants could imply that Idgfs function as growth hormones; loss of function could slow
444 development. Nevertheless, we found no significant size difference between *Idgf* mutants and controls.

445 Consistent with disruption of embryonic development (as revealed by lower *sxtΔ* hatch rates), we
446 observed abnormal expression of Engrailed protein and disorganized denticle belts in embryos, including
447 a mislocalization of Engrailed at the cell membrane. Patterning is achieved through the expression of
448 the segment polarity genes *wingless* (*wg*) and *engrailed* (*en*), which activates expression of *hedgehog*
449 (*hh*). Within each segment, cells receiving the Wg signal produce smooth cuticle posteriorly, and cells
450 receiving the Hh signal produce denticles anteriorly (BEJSOVEC AND MARTINEZ ARIAS 1991; SWARUP AND
451 VERHEYEN 2012). The denticle-versus-smooth cell shapes are distinct: whereas the denticle-producing
452 cells are rectangular and arranged in rows with the long edges oriented in the ventrolateral direction
453 (similar to a staggered brick-wall arrangement), the smooth cells are larger and not arranged in rows
454 (HIRANO *et al.* 2009). Mislocalization or abnormal expression of En could cause a transformation of cell
455 fate from non-denticle-producing to denticle-producing cells, resulting in the disorganized denticle belt
456 phenotype we observed in *sxtΔ* embryos (Figure S4B). Alternatively, cells in the epidermal epithelium
457 may have altered cell adhesion and increased motility, allowing denticle-producing cells to invade into
458 the non-denticle-producing cells.

459 Segmentation defects were apparent in adults in that *sxtΔ* flies exhibited etched tergites. Each
460 abdominal segment in the adult epidermis develops from three bilateral pairs of groups of cells called
461 histoblast nests. The anterior pair in each segment forms the tergite. Histoblast nests proliferate after
462 pupariation and migrate by intercalation into the larval epithelial cells, which then extrude basally and
463 die. The histoblast nests fuse and secrete the adult cuticle (ATHILINGAM *et al.* 2021; DAVIS *et al.* 2022;
464 MANGIONE AND MARTIN-BLANCO 2018; MICHEL AND DAHMANN 2020; NARDI *et al.* 2018; PANZADE AND MATIS
465 2021; PRAT-ROJO *et al.* 2020). Successful migration depends on Decapentaplegic (Dpp) and protrusive
466 extensions at the leading edge of the histoblast nests (NINOV *et al.* 2007; NINOV *et al.* 2010). Our findings
467 suggest a role for Idgfs in cell migration, but how Idgfs function in tergite formation is unknown.

468 Our previous studies showed that the stretch cells relay signals from the nurse cells to the DA cells to
469 guide their movement and ensure tube closure. These signals rely on function of the SOX transcription
470 factor Bullwinkle (Bwk) in the nurse cells [Rittenhouse dissertation, 1996. Bullwinkle, an HMG box
471 protein, is required for proper development during oogenesis, embryogenesis and metamorphosis in
472 *Drosophila melanogaster*, PhD, University of Washington; (RITTENHOUSE AND BERG 1995)], and the non-
473 receptor tyrosine kinases Shark and Src42a in the stretch cells (TRAN AND BERG 2003). The specific
474 signaling molecules and their targets are unknown. *Bwk* mutants produce short, wide, open tubes that
475 create DAs resembling moose antlers (DORMAN *et al.* 2004; RITTENHOUSE AND BERG 1995). Shark and
476 Src42A act downstream of Bwk to regulate DA morphogenesis; Shark loss of function enhances the Bwk
477 phenotype (TRAN AND BERG 2003).

478 In this study, we found that except for *Idgf6*, the single *Idgf*-null mutants did not cause a defective DA
479 phenotype. The results for the single null mutants contrast with our previous studies using RNAi to
480 knock down each *Idgf* individually (ZIMMERMAN *et al.* 2017); we found that RNAi knockdown of each *Idgf*
481 results in a partially penetrant DA phenotype featuring shorter, wider DAs. Shorter, wider DAs also
482 occur when Idgfs are overexpressed or elevated as in eggs from *bwk* mutant flies and contrast with the
483 moderate category of defective DAs in the null mutants, which have thin DAs. Why do significant
484 defects occur in single *Idgf* RNAi knockdowns, but not in single nulls? Functional redundancy from the
485 remaining Idgfs or even from non-Idgf genes could account for the incomplete penetrance or lack of a

486 phenotype. Duplicated genes can maintain functional redundancy despite their divergence over
487 evolutionary time (DEAN *et al.* 2008; DELUNA *et al.* 2008; KAFRI *et al.* 2008; MUSSO *et al.* 2008). Functional
488 redundancy between paralogous genes can result in a strong phenotype when all of the paralogs are
489 deleted and a weak or neutral phenotype when the genes are deleted singly (DEAN *et al.* 2008; DELUNA *et*
490 *al.* 2008; GU *et al.* 2003; KAFRI *et al.* 2008; MUSSO *et al.* 2008), similar to what we observed for the *Idgf*
491 null mutants.

492 Compensation in single null mutants from the remaining wild-type paralogs or even from non-*Idgf* genes
493 could be post-transcriptional, e.g., through increased translation or greater protein stability.
494 Compensation may also occur through transcriptional adaptation, in which upregulation of
495 compensating genes can be triggered by any of a number of mRNA decay pathways that target aberrant
496 mRNAs (GARNEAU *et al.* 2007). A recent study demonstrated that transcriptional adaptation depends on
497 the existence of a mutant mRNA, for which degradation can occur via different surveillance pathways,
498 including non-stop, no-go, or nonsense-mediated decay, depending on the nature of the mutation.
499 Upregulation can then occur in genes with sequence similarity to the degraded mRNA (EL-BROLOSY *et al.*
500 2019; EL-BROLOSY AND STAINIER 2017; GARNEAU *et al.* 2007; ROSSI *et al.* 2015).

501 Except for *Idgf2Δ*, the single null mutants cannot express a transcript. The *Idgf2* deletion leaves intact
502 the 5' UTR, the first exon and intron, and part of the second exon, potentially allowing production of a
503 mutant transcript and therefore transcriptional adaptation in the *Idgf2Δ* and *sxtΔ* mutants, which carry
504 the *Idgf2* deletion. Degradation of the *Idgf2Δ* transcript could not be via the nonsense-mediated decay
505 (NMD) process, which requires a premature stop codon upstream of an intron. Degradation via a non-
506 NMD pathway, however, could be occurring in either the $Idgf^{2\Delta}$ or *sxtΔ* mutant lines. Our RNAi
507 experiments were performed in a wild-type background, so there would be no mutant mRNAs, and any
508 adaptation would be on the translational or post-translational protein level (DELUNA *et al.* 2010;
509 DONNELLY AND STORCHOVA 2014; ISHIKAWA *et al.* 2017; TORRES *et al.* 2008).

510 Although adaptation could be occurring in both the nulls and the knockdowns, the time frame for
511 adaptation could also be a factor. In the RNAi study, we used the GAL4/UAS system to knockdown
512 transcripts from each of the *Idgf* genes. We used a stretch-cell-specific Gal4 driver, which is not
513 expressed until Stage 10 of egg chamber development, after patterning has occurred but just hours
514 before tube formation. This timing may not allow enough time for compensation to occur. On the other
515 hand, *Idgf*-null mutant flies are mutant throughout their entire life cycle. Thus, the different results of
516 our *Idgf* RNAi knockdown and null experiments could be due to different mechanisms of compensation.
517 Discerning whether compensation is occurring and what contributes to the differences in phenotypes
518 exhibited by overexpression, RNAi, and gene deletion will require further study.

519 Mutations can render cells less robust to endogenous or exogenous perturbations (LEVY AND SIEGAL 2008;
520 MASEL AND SIEGAL 2009). *Drosophila* researchers commonly use CO_2 to anesthetize flies without
521 considering the potential profound and long-lasting effects of CO_2 exposure. Previous studies have
522 shown that hypercapnia can suppress the immune system and alter gene expression via the NF-κB
523 pathway in mammalian cells (CUMMINS *et al.* 2010). Hypercapnia also reduces fertility (HELENIUS *et al.*
524 2009) and alters climbing and flight behavior in *Drosophila* (BARTHOLOMEW *et al.* 2015).

525 We demonstrated that exposing *Idgf*-null mutants to CO_2 enhances dorsal appendage morphogenesis
526 defects independently of hypoxia and induces loss of cortical Actin in epithelial tissues during oogenesis
527 and embryonic development. We did note molecular differences, raising the question of whether Idgfs

528 regulate E-cadherin in normoxia and Actin in response to CO_2. We saw that E-cadherin was disrupted in
529 *sxtΔ* mutant egg chambers but was unaffected by CO_2 exposure in either egg chambers or embryos. In
530 contrast, Actin levels were unaffected in *sxtΔ* mutants vs. controls but significantly reduced in *sxtΔ*
531 mutants upon CO_2 exposure. It could be that the Actin is also perturbed in wild-type tissue but recovers,
532 whereas absence of Idgfs eliminates a similar recovery in *sxtΔ* tissue. The mechanisms leading to these
533 novel outcomes are unknown.

534 One possible mechanism for this regulation is that Idgfs interact with the immune deficiency (IMD)
535 pathway through the transcription factor Relish (Drosophila NF-κB). Previous studies show that Relish
536 inhibits JNK signaling (Park et al., 2004). Activation of JNK signaling reorganizes the Actin cytoskeleton,
537 impacting developmental processes such as cell migration and dorsal closure (HOMSY *et al.* 2006; JACINTO
538 *et al.* 2000; KALTSCHMIDT *et al.* 2002; KOCKEL *et al.* 2001; RUDRAPATNA *et al.* 2014). Upon Relish loss, JNK
539 activation causes upregulation of actin remodelers (RAMESH *et al.* 2021). Another possibility is that CO_2
540 exposure reduces pH at the cell membrane, thereby altering Actin dynamics. pH is an important
541 regulator in developmental processes such as differentiation (ULMSCHNEIDER *et al.* 2016) and tissue
542 architecture (GRILLO-HILL *et al.* 2015). Alternatively, the mechanism could involve a pathway
543 independent of JNK signaling or pH.

544 A common thread among the various phenotypes produced by loss of all Idgfs is the disruption of E-
545 cadherin and Actin, an outcome that could interfere with cell migration, segmentation, and tissue
546 morphogenesis. Consistent with this hypothesis, we recently identified eukaryotic translation initiation
547 factor 3 subunit e (eIF3e) as a strong enhancer of Idgf3 overexpression (ESPINOZA AND BERG 2020). eIF3e
548 is part of a complex that regulates the redox enzyme, Mical, which functions to disassemble Actin
549 filaments and inhibit Actin polymerization (GRINTSEVICH *et al.* 2021; GRINTSEVICH *et al.* 2017; GRINTSEVICH *et*
550 *al.* 2016; HUNG *et al.* 2010). We are currently beginning to investigate the mechanistic role of Idgfs in
551 this pathway.

552 Our investigation into the effects of complete loss of function of Idgfs has raised intriguing questions
553 regarding Idgf function. What are the pathways? What are the precise mechanisms? What are the
554 common threads among the various phenotypes? Our *Idgf* null lines are valuable tools that will
555 facilitate studies providing new insights into the function of Idgfs in *Drosophila*. Our results suggest new
556 avenues of investigation for the mechanisms of CLP function in cancer pathogenesis, autoimmune
557 disease, and tissue remodeling disorders.

558

559 Materials and Methods

560 Fly stocks

561 Bloomington stocks: w^{1118} (3605), *Df(2L)ED1102* (24113), *Df(1)ED6989* (9056), *Df(2R)BSC337* (24361),
562 Df(2R)Exel6064 (7546). VDRC stock: Idgf6$^{fTRG01331.sfGFP\text{-}TVPTBF}$ (SAROV *et al.* 2016). Stocks generated in this
563 study: $Idgf^{1\Delta}$, $Idgf^{2\Delta}$, $Idgf^{3\Delta}$, $Idgf^{4\Delta}$, $Idgf^{5\Delta}$, $Idgf^{6\Delta}$, and Idgf$^{4\Delta}$; Idgfp$^{(1\text{-}3)\Delta,(6\text{-}5)\Delta}$ (*sxtΔ*) were used in the
564 experiments. All *Idgf* mutants generated in this study, including double and triple nulls, are listed in
565 Table S2. Flies were maintained on standard molasses food at 25°C.

566 **Reagents and materials**

567 <u>Ovaries</u>

568 - Dissecting dishes and forceps

- PBS, 10x (Sambrook et al. 1989), NaCl 80 g, KCl 2 g, Na2HPO4 14.4 g, KH2PO4 2.4 g in 1 L of H2O pH 7.4.
- PBT, 0.1% (vol/vol) Tween 20 diluted in 1× PBS
- EBR, 10× (modified Ephrussi-Beadle Ringer's solution) 1.3 M NaCl, 47 mM KCl, 19 mM CaCl2 and 100 mM HEPES (pH 6.9).
- Paraformaldehyde, 4% (wt/vol), Dilute 16% (wt/vol) paraformaldehyde in 1× PBS at a ratio of 1:4
- Western Blocking Reagent (WBR)

<u>Embryos</u>

- Flow Buddy - Benchtop Flow Regulator (Genesee Cat #: 59-122B)
- Egg collection basket - Falcon tube (50 mL) with the bottom cut off and nylon mesh attached to bottom (e.g., melt the bottom edge slightly with a Bunsen burner and press on the nylon mesh)
- Double-sided sticky tape
- Whatman paper
- Pipette controller (e.g., Millipore Sigma BR25900)
- Pasteur pipettes, glass, 3.5 inches
- Petri dish lid
- Plastic fly bottles punched with holes (to make egg laying chambers when attached to apple juice plates)
- 30G syringe needles + plastic syringes
- PBTA with 0.05% or 0.1% Triton (1x PBS, 1% BSA, 0.05% or 0.1% Triton X-100, 0.02% Sodium Azide)
- Apple juice plates, 175 mL H_2O, 25 mL 4x apple juice, 5 g of agar 1.2 g of methyl paraben. Heat in microwave until agar dissolves. Pour into Petri dish lids. These will be attached to the plastic fly bottles using rubber bands.
- Bleach
- Heptane Saturated with 37% Formaldehyde - Combine equal volumes of heptane and 37% formaldehyde, shake the mixture vigorously for 15 seconds. Let the solution settle into the 2 phases. Prepare the solution the day before it is to be used, shaking the vial or bottle periodically throughout the day. The saturated heptane is the upper phase in the 1:1 heptane:formaldehyde stock. Store at room temperature, protected from light, up to several months.
- 1x Embryo Wash Solution, - 0.7% NaCl, 0.05% Triton X-100, H_2O
- Normal goat serum (NGS)

Tissue processing and Immunohistochemistry

Ovaries - Ovaries were dissected in EBR, fixed for 20 minutes in 4% (wt/vol) paraformaldehyde, permeabilized for 1 hour in 1% PBS-Triton, and blocked for 1 hour in WBR. Primary antibodies: mouse anti-Broad (1:500), rat anti-Ecadherin (1:50) (DSHB DCAD2), rabbit anti-Vasa (1:2000) (Paul Lasko) (Figure S2A), rat anti-Vasa (1:500) (Figure S3), mouse anti-Engrailed concentrate (1:20) or supernatant (1:50) (DSHB 4D9). Secondary antibodies: Alexa Fluor goat anti-mouse (1:200) and goat anti-rat (1:200). Ovaries were washed in PBT, incubated O/N at 4°C in PBT with primary antibodies and 5% NGS, washed

611 in PBT, incubated for 1 hour at room temperature in secondary antibodies and DAPI, washed in PBT,
612 mounted on slides and imaged on a Leica SP8X LSM.

613 Embryos - Females were aged for 2 days with wet yeast paste. ~100 males and ~100 females were
614 mated and allowed to lay on apple juice plates O/N or for a few hours to obtain a range of desired
615 stages. All aspects of this experiment prior to dechorionization were done at 25°C. Embryos were
616 exposed to either 100% CO_2 or air for 2 minutes by inserting the CO_2 needle through a hole in the plastic
617 fly bottle. The CO_2 or air was humidified by flowing the gas through a bubbler and the flow rate was
618 held precisely at 3.5 L per minute, using the Flow Buddy. Using a paint brush and embryo wash,
619 embryos were washed from plates into a basket and rinsed with embryo wash using a squirt bottle, then
620 dechorionated in 50% bleach (1:1 bleach:H_2O) for 2 minutes by submerging the mesh end of the basket
621 in a Falcon tube with the bleach. The de-chorionated embryos were rinsed with embryo wash in the
622 basket, then transferred to a 1.5 mL Eppendorf tube by squirting embryo wash onto the outside end of
623 the mesh and into the Eppendorf tube. Embryos were fixed for 40 minutes in 1 mL of heptane saturated
624 with 37% formaldehyde. Using a pipette tip with the tip cut off and pre-treated in PBTA, embryos were
625 transferred to Whatman paper for ~30 seconds to allow the heptane to evaporate. The Whatman paper
626 was placed embryo side down on the tape, gently tapped until embryos were stuck to the tape, and the
627 embryos were immediately covered with PBS. Vitelline membranes were manually removed using 30-
628 Gauge syringe needles. Using a pipette controller attached to a glass Pasteur pipette pre-treated with
629 PBTA, embryos were transferred to PBTA with 0.1% Triton X-100 for staining or to PBTA with 0.05%
630 Triton X-100 for storage at 4°C. Stage 3-5 embryos were incubated with DAPI (1µg/mL), and rhodamine
631 phalloidin (Abcam ab235138) (1:500) for 1 hour, and washed in PBTA with 0.05% Triton X-100 for 1
632 hour, rinsed 3x in PBS, and mounted in Vectashield mounting medium. Stage 8-12 embryos were
633 incubated with rat anti-E-cadherin (1:50) and mouse anti-Engrailed concentrate (1:20) or supernatant
634 (1:50) in PBTA with 0.1% Triton X-100 and NGS O/N at 4°C, washed for 1 hour in PBTA with 0.1% Triton
635 X-100, incubated for 1 hour at RT in PBTA with 0.1% Triton X-100, 5% NGS, DAPI (1µg/mL), rhodamine
636 phalloidin (Abcam ab235138) (1:500), Alexa Fluor goat anti-mouse 488 and anti-rat 647, washed for 1
637 hour in PBTA with 0.1% Triton X-100, rinsed 3x in PBS, and mounted on slides with Vectashield mounting
638 medium.

639 **Generation of *Idgf* mutant fly lines**

640 Deletions of the entire locus or most of the locus for each of *Idgf1*, *Idgf2*, *Idgf3*, *Idgf4*, *Idgf5*, and *Idgf6*
641 were created using CRISPR/Cas9-catalyzed homology-directed repair. For each deletion, we designed
642 and injected three vectors: two guide RNAs and one donor containing a Ds-Red eye reporter to aid in
643 screening newly transformed flies. Using the FlyCRISPR algorithm
644 (tools.flycrispr.molbio.wisc.edu/targetFinder), we designed guide RNAs targeting sites upstream and
645 downstream of each gene. Guide RNAs were synthesized as 5'-phosphorylated oligos (Operon),
646 annealed, and ligated into the BbsI sites of the pU6-BbsI-chiRNA plasmid (Addgene #45946). For the
647 donor vector, we PCR amplified ~1kb homology arms from genomic DNA of the injection strain and
648 cloned them into pHD-DsRed-attP (Addgene #51019). We co-injected guide RNAs and donor vectors
649 (Rainbow Transgenics) into *y vas-Cas9* w^{1118} embryos (Bloomington 55821) and screened F1 flies for
650 germline transmission of the DsRed reporter, followed by single-fly PCR and sequencing. The *Idgf* null
651 strains were outcrossed to w^{1118}*; +; +* for three generations to remove background effects and remove
652 the *vas-Cas9* transgene. All of the single *Idgf*-null lines are homozygous viable and fertile.

653 **Image analysis and quantification**

654 For egg chambers, images were acquired as 8-bit images at the same laser intensities and detector
655 settings on a Leica SP8X LSM. Using ImageJ, we measured E-cadherin and Actin intensity across three
656 cell membranes, from the center of one cell to the center of the neighboring cell, in at least 6 egg
657 chambers for each genotype and compared egg chambers exposed to CO_2 to egg chambers not exposed
658 to CO_2. Plot profiles across 5.0 µm were averaged over all egg chambers for each genotype and
659 treatment.

660 For embryos, images of all genotypes and treatments were acquired as 16-bit images at the same laser
661 intensities and detector settings on a Leica SP8X LSM. For each individual channel and optical plane
662 being measured, background was subtracted, and a median filter was applied (rolling ball radius of 2.0)
663 prior to measurements. For each genotype, we measured E-cadherin and Actin fluorescent intensity as
664 above, across 6 cell membranes per embryo, with n=10 embryos for each treatment (no CO_2, +CO_2, and
665 +air) within three bioreplicates, except for *sxtΔ* bioreplicate 3, no CO_2 (n=6 embryos). Plot profiles across
666 3.5 µm were averaged over all embryos for each genotype and treatment. Total E-cadherin or Actin was
667 calculated by integrating the area under the mean plot profile curve using the trapezoidal rule. Data
668 analyses were performed in Excel. Statistical analyses were performed in Excel and R.

669

670 Data Availability

671 Fly lines are available upon request. The authors affirm that all data necessary for confirming the
672 conclusions of the article are present within the article, figures, tables, and in the supplementary data
673 files: Data Files S1 through S8. Data file S1 contains hatch rate data, data file S2 contains dorsal
674 appendage defect and rescue data, data file S3 contains hypoxia and CO_2 exposure data, data file S4
675 contains Actin and E-cadherin profile data for egg chambers, data file S5 contains Actin and E-cadherin
676 profile data in later stage embryos, data file S6 contains Actin and E-cadherin profile data in earlier stage
677 embryos, data file S7 contains eclosion data, and data file S8 contains germ-cell count data.

678 Acknowledgements

679 We thank the Bloomington *Drosophila* Stock Center (NIH P40OD018537) and the Vienna *Drosophila*
680 Resource Center for stocks, and FlyBase for genetic, polypeptide, and functional data. The rabbit anti-
681 Vasa antibody (Liu *et al.* 2009) was a gift from Paul Lasko. The mouse anti-Broad, rat anti-Vasa, and rat
682 anti-E-cadherin antibodies were obtained from the Developmental Studies Hybridoma Bank, created by
683 the National Institute of Child Health and Human Development of the National Institutes of Health (NIH)
684 and maintained by the University of Iowa, Department of Biology. We thank Nathaniel Peters at the
685 University of Washington Keck Center for technical support and advice on imaging. We thank Vincent So
686 for providing the data and image for Idgf6::GFP localization to germ cells. We thank Dana Miller in the
687 Department of Biochemistry at the University of Washington for technical assistance and advice on the
688 hypoxia and CO_2 experiments and Greg Beitel in the Department of Molecular Biosciences at
689 Northwestern University for technical assistance and advice on the CO_2 experiments.

690

691 # Funding
692 NIH R01 GM079433

693 # Author Contributions
694 Celeste Berg – Project design; oversight of all experiments; analysis of mutant embryos; review and
695 editing of manuscript

696 Liesl Strand – Generation of *Idgf6Δ* fly strain using CRISPR/Cas9; experiments and data analysis to
697 examine *Idgf6Δ* dorsal appendage defects; experiments to assess variability in phenotypes; review of
698 manuscript.

699 Anne Sustar – Generation of *Idgf* null fly strains using CRISPR/Cas9; experiments (hatch rates, dorsal
700 appendage morphogenesis, adult phenotype analysis, germ cell migration phenotype, CO_2 response in
701 egg chambers, patterning in egg chambers, Actin and E-cadherin measurements in egg chambers);
702 imaging; data analyses; review of manuscript.

703 Sandra Zimmerman – writing and editing drafts, constructing figures, experiments (E-cadherin and Actin
704 in embryos, hatch rates), imaging, and data analysis.

705

706 # Competing Interests
707 The authors declare no competing interests.

708

709 # References
710 ARESHKOV, P. O., S. S. AVDIEIEV, O. V. BALYNSKA, D. LEROITH AND V. M. KAVSAN, 2012 Two closely related
711 human members of chitinase-like family, CHI3L1 and CHI3L2, activate ERK1/2 in 293 and U373
712 cells but have the different influence on cell proliferation. Int J Biol Sci **8:** 39-48.
713 ARIAS, E. B., H. G. VERHAGE AND R. C. JAFFE, 1994 Complementary deoxyribonucleic acid cloning and
714 molecular characterization of an estrogen-dependent human oviductal glycoprotein. Biol
715 Reprod **51:** 685-694.
716 ATHILINGAM, T., P. TIWARI, Y. TOYAMA AND T. E. SAUNDERS, 2021 Mechanics of epidermal morphogenesis in
717 the Drosophila pupa. Semin Cell Dev Biol **120:** 171-180.
718 BARTHOLOMEW, N. R., J. M. BURDETT, J. M. VANDENBROOKS, M. C. QUINLAN AND G. B. CALL, 2015 Impaired
719 climbing and flight behaviour in Drosophila melanogaster following carbon dioxide anaesthesia.
720 Sci Rep **5:** 15298.
721 BEJSOVEC, A., AND A. MARTINEZ ARIAS, 1991 Roles of wingless in patterning the larval epidermis of
722 Drosophila. Development **113:** 471-485.
723 BROWN, S., M. P. ZEIDLER AND J. E. HOMBRIA, 2006 JAK/STAT signalling in Drosophila controls cell motility
724 during germ cell migration. Dev Dyn **235:** 958-966.
725 BROZ, V., L. KUCEROVA, L. ROUHOVA, J. FLEISCHMANNOVA, H. STRNAD *et al.*, 2017 Drosophila imaginal disc
726 growth factor 2 is a trophic factor involved in energy balance, detoxification, and innate
727 immunity. Sci Rep **7:** 43273.
728 CARTON, Y., AND A. J. NAPPI, 2001 Immunogenetic aspects of the cellular immune response of Drosophilia
729 against parasitoids. Immunogenetics **52:** 157-164.

730 CUMMINS, E. P., K. M. OLIVER, C. R. LENIHAN, S. F. FITZPATRICK, U. BRUNING *et al.*, 2010 NF-kappaB links CO2
731 sensing to innate immunity and inflammation in mammalian cells. J Immunol **185:** 4439-4445.
732 DAVIS, J. R., A. P. AINSLIE, J. J. WILLIAMSON, A. FERREIRA, A. TORRES-SANCHEZ *et al.*, 2022 ECM degradation in
733 the Drosophila abdominal epidermis initiates tissue growth that ceases with rapid cell-cycle exit.
734 Curr Biol **32:** 1285-1300 e1284.
735 DEAN, E. J., J. C. DAVIS, R. W. DAVIS AND D. A. PETROV, 2008 Pervasive and persistent redundancy among
736 duplicated genes in yeast. PLoS Genet **4:** e1000113.
737 DELUNA, A., M. SPRINGER, M. W. KIRSCHNER AND R. KISHONY, 2010 Need-based up-regulation of protein levels
738 in response to deletion of their duplicate genes. PLoS Biol **8:** e1000347.
739 DELUNA, A., K. VETSIGIAN, N. SHORESH, M. HEGRENESS, M. COLON-GONZALEZ *et al.*, 2008 Exposing the fitness
740 contribution of duplicated genes. Nat Genet **40:** 676-681.
741 DI ROSA, M., G. DISTEFANO, K. ZORENA AND L. MALAGUARNERA, 2016 Chitinases and immunity: Ancestral
742 molecules with new functions. Immunobiology **221:** 399-411.
743 DILKS, S. A., AND S. DINARDO, 2010 Non-cell-autonomous control of denticle diversity in the Drosophila
744 embryo. Development **137:** 1395-1404.
745 DONNELLY, N., AND Z. STORCHOVA, 2014 Dynamic karyotype, dynamic proteome: buffering the effects of
746 aneuploidy. Biochim Biophys Acta **1843:** 473-481.
747 DORMAN, J. B., K. E. JAMES, S. E. FRASER, D. P. KIEHART AND C. A. BERG, 2004 *bullwinkle* is required for
748 epithelial morphogenesis during *Drosophila* oogenesis. Dev Biol **267:** 320-341.
749 EL-BROLOSY, M. A., Z. KONTARAKIS, A. ROSSI, C. KUENNE, S. GUNTHER *et al.*, 2019 Genetic compensation
750 triggered by mutant mRNA degradation. Nature **568:** 193-197.
751 EL-BROLOSY, M. A., AND D. Y. R. STAINIER, 2017 Genetic compensation: A phenomenon in search of
752 mechanisms. PLoS Genet **13:** e1006780.
753 ESPINOZA, C. Y., AND C. A. BERG, 2020 Detecting New Allies: Modifier Screen Identifies a Genetic Interaction
754 Between Imaginal disc growth factor 3 and combover, a Rho-kinase Substrate, During Dorsal
755 Appendage Tube Formation in Drosophila. G3 (Bethesda) **10:** 3585-3599.
756 FRANCESCONE, R. A., S. SCULLY, M. FAIBISH, S. L. TAYLOR, D. OH *et al.*, 2011 Role of YKL-40 in the angiogenesis,
757 radioresistance, and progression of glioblastoma. J Biol Chem **286:** 15332-15343.
758 FUHRMAN, J. A., W. S. LANE, R. F. SMITH, W. F. PIESSENS AND F. B. PERLER, 1992 Transmission-blocking
759 antibodies recognize microfilarial chitinase in brugian lymphatic filariasis. Proc Natl Acad Sci U S
760 A **89:** 1548-1552.
761 FUSETTI, F., T. PIJNING, K. H. KALK, E. BOS AND B. W. DIJKSTRA, 2003 Crystal structure and carbohydrate-
762 binding properties of the human cartilage glycoprotein-39. J Biol Chem **278:** 37753-37760.
763 GARNEAU, N. L., J. WILUSZ AND C. J. WILUSZ, 2007 The highways and byways of mRNA decay. Nat Rev Mol
764 Cell Biol **8:** 113-126.
765 GLOVER, D. M., AND B. D. HAMES, 1989 *Genes and embryos*. IRL Press, Oxford ; New York.
766 GRILLO-HILL, B. K., C. CHOI, M. JIMENEZ-VIDAL AND D. L. BARBER, 2015 Increased H(+) efflux is sufficient to
767 induce dysplasia and necessary for viability with oncogene expression. Elife **4**.
768 GRINTSEVICH, E. E., G. AHMED, A. A. GINOSYAN, H. WU, S. K. RICH *et al.*, 2021 Profilin and Mical combine to
769 impair F-actin assembly and promote disassembly and remodeling. Nat Commun **12:** 5542.
770 GRINTSEVICH, E. E., P. GE, M. R. SAWAYA, H. G. YESILYURT, J. R. TERMAN *et al.*, 2017 Catastrophic disassembly of
771 actin filaments via Mical-mediated oxidation. Nat Commun **8:** 2183.
772 GRINTSEVICH, E. E., H. G. YESILYURT, S. K. RICH, R. J. HUNG, J. R. TERMAN *et al.*, 2016 F-actin dismantling
773 through a redox-driven synergy between Mical and cofilin. Nat Cell Biol **18:** 876-885.
774 GU, Z., L. M. STEINMETZ, X. GU, C. SCHARFE, R. W. DAVIS *et al.*, 2003 Role of duplicate genes in genetic
775 robustness against null mutations. Nature **421:** 63-66.

776 GUAN, R., R. LIN, R. JIN, L. LU, X. LIU *et al.*, 2020 Chitinase-like protein YKL-40 regulates human bronchial
777 epithelial cells proliferation, apoptosis, and migration through TGF-beta1/Smads pathway. Hum
778 Exp Toxicol **39:** 451-463.
779 HANYU-NAKAMURA, K., S. KOBAYASHI AND A. NAKAMURA, 2004 Germ cell-autonomous Wunen2 is required for
780 germline development in Drosophila embryos. Development **131:** 4545-4553.
781 HE, C. H., C. G. LEE, C. S. DELA CRUZ, C. M. LEE, Y. ZHOU *et al.*, 2013 Chitinase 3-like 1 regulates cellular and
782 tissue responses via IL-13 receptor alpha2. Cell Rep **4:** 830-841.
783 HELENIUS, I. T., R. J. HAAKE, Y. J. KWON, J. A. HU, T. KRUPINSKI *et al.*, 2016 Identification of Drosophila Zfh2 as
784 a Mediator of Hypercapnic Immune Regulation by a Genome-Wide RNA Interference Screen. J
785 Immunol **196:** 655-667.
786 HELENIUS, I. T., T. KRUPINSKI, D. W. TURNBULL, Y. GRUENBAUM, N. SILVERMAN *et al.*, 2009 Elevated CO2
787 suppresses specific Drosophila innate immune responses and resistance to bacterial infection.
788 Proc Natl Acad Sci U S A **106:** 18710-18715.
789 HIRANO, M., D. NEFF AND S. COLLIER, 2009 Cell shape and epithelial patterning in the Drosophila embryonic
790 epidermis. Fly (Austin) **3:** 185-191.
791 HOMSY, J. G., H. JASPER, X. G. PERALTA, H. WU, D. P. KIEHART *et al.*, 2006 JNK signaling coordinates integrin
792 and actin functions during Drosophila embryogenesis. Dev Dyn **235:** 427-434.
793 HU, B., K. TRINH, W. F. FIGUEIRA AND P. A. PRICE, 1996 Isolation and sequence of a novel human chondrocyte
794 protein related to mammalian members of the chitinase protein family. J Biol Chem **271:** 19415-
795 19420.
796 HUNG, R.-J., U. YAZDANI, J. YOON, H. WU, T. YANG *et al.*, 2010 Mical links semaphorins to F-actin
797 disassembly. Nature **463:** 823-827.
798 IRVING, P., L. TROXLER, T. S. HEUER, M. BELVIN, C. KOPCZYNSKI *et al.*, 2001 A genome-wide analysis of immune
799 responses in Drosophila. Proc Natl Acad Sci U S A **98:** 15119-15124.
800 ISHIKAWA, K., K. MAKANAE, S. IWASAKI, N. T. INGOLIA AND H. MORIYA, 2017 Post-Translational Dosage
801 Compensation Buffers Genetic Perturbations to Stoichiometry of Protein Complexes. PLoS Genet
802 **13:** e1006554.
803 JACINTO, A., W. WOOD, T. BALAYO, M. TURMAINE, A. MARTINEZ-ARIAS *et al.*, 2000 Dynamic actin-based
804 epithelial adhesion and cell matching during Drosophila dorsal closure. Curr Biol **10:** 1420-1426.
805 KAFRI, R., O. DAHAN, J. LEVY AND Y. PILPEL, 2008 Preferential protection of protein interaction network hubs
806 in yeast: evolved functionality of genetic redundancy. Proc Natl Acad Sci U S A **105:** 1243-1248.
807 KALTSCHMIDT, J. A., N. LAWRENCE, V. MOREL, T. BALAYO, B. G. FERNANDEZ *et al.*, 2002 Planar polarity and actin
808 dynamics in the epidermis of Drosophila. Nat Cell Biol **4:** 937-944.
809 KAWAMURA, K., T. SHIBATA, O. SAGET, D. PEEL AND P. J. BRYANT, 1999 A new family of growth factors produced
810 by the fat body and active on *Drosophila* imaginal disc cells. Development **126:** 211-219.
811 KHUSH, R. S., AND B. LEMAITRE, 2000 Genes that fight infection: what the Drosophila genome says about
812 animal immunity. Trends Genet **16:** 442-449.
813 KIRKPATRICK, R. B., R. E. MATICO, D. E. MCNULTY, J. E. STRICKLER AND M. ROSENBERG, 1995 An abundantly
814 secreted glycoprotein from *Drosophila melanogaster* is related to mammalian secretory proteins
815 produced in rheumatoid tissues and by activated macrophages. Gene **153:** 147-154.
816 KOCKEL, L., J. G. HOMSY AND D. BOHMANN, 2001 Drosophila AP-1: lessons from an invertebrate. Oncogene
817 **20:** 2347-2364.
818 KUCEROVA, L., V. BROZ, B. AREFIN, H. O. MAAROUFI, J. HURYCHOVA *et al.*, 2016 The *Drosophila* chitinase-like
819 protein IDGF3 is involved in protection against nematodes and in wound healing. J Innate
820 Immun **8:** 199-210.
821 KUNWAR, P. S., H. SANO, A. D. RENAULT, V. BARBOSA, N. FUSE *et al.*, 2008 Tre1 GPCR initiates germ cell
822 transepithelial migration by regulating Drosophila melanogaster E-cadherin. J Cell Biol **183:** 157-
823 168.

824 KUNWAR, P. S., M. STARZ-GAIANO, R. J. BAINTON, U. HEBERLEIN AND R. LEHMANN, 2003 Tre1, a G protein-
825 coupled receptor, directs transepithelial migration of Drosophila germ cells. PLoS Biol **1:** E80.
826 KZHYSHKOWSKA, J., A. GRATCHEV, J. H. MARTENS, O. PERVUSHINA, S. MAMIDI *et al.*, 2004 Stabilin-1 localizes to
827 endosomes and the trans-Golgi network in human macrophages and interacts with GGA
828 adaptors. J Leukoc Biol **76:** 1151-1161.
829 KZHYSHKOWSKA, J., S. MAMIDI, A. GRATCHEV, E. KREMMER, C. SCHMUTTERMAIER *et al.*, 2006 Novel stabilin-1
830 interacting chitinase-like protein (SI-CLP) is up-regulated in alternatively activated macrophages
831 and secreted via lysosomal pathway. Blood **107:** 3221-3228.
832 KZHYSHKOWSKA, J., S. YIN, T. LIU, V. RIABOV AND I. MITROFANOVA, 2016 Role of chitinase-like proteins in
833 cancer. Biol Chem **397:** 231-247.
834 LEBLANC, M. G., AND R. LEHMANN, 2017 Domain-specific control of germ cell polarity and migration by
835 multifunction Tre1 GPCR. J Cell Biol **216:** 2945-2958.
836 LEE, C. G., C. A. DA SILVA, C. S. DELA CRUZ, F. AHANGARI, B. MA *et al.*, 2011 Role of chitin and
837 chitinase/chitinase-like proteins in inflammation, tissue remodeling, and injury. Annu Rev
838 Physiol **73:** 479-501.
839 LEVY, S. F., AND M. L. SIEGAL, 2008 Network hubs buffer environmental variation in Saccharomyces
840 cerevisiae. PLoS Biol **6:** e264.
841 LI, J., F. XIA AND W. X. LI, 2003 Coactivation of STAT and Ras is required for germ cell proliferation and
842 invasive migration in Drosophila. Dev Cell **5:** 787-798.
843 LIBREROS, S., R. GARCIA-AREAS, P. KEATING, R. CARRIO AND V. L. IRAGAVARAPU-CHARYULU, 2013 Exploring the role
844 of CHI3L1 in "pre-metastatic" lungs of mammary tumor-bearing mice. Front Physiol **4:** 392.
845 LIU, N., H. HAN AND P. LASKO, 2009 Vasa promotes Drosophila germline stem cell differentiation by
846 activating mei-P26 translation by directly interacting with a (U)-rich motif in its 3' UTR. Genes
847 Dev **23:** 2742-2752.
848 LOW, D., R. SUBRAMANIAM, L. LIN, T. AOMATSU, A. MIZOGUCHI *et al.*, 2015 Chitinase 3-like 1 induces survival
849 and proliferation of intestinal epithelial cells during chronic inflammation and colitis-associated
850 cancer by regulating S100A9. Oncotarget **6:** 36535-36550.
851 LU, Y., N. CHANG, X. ZHAO, R. XUE, J. LIU *et al.*, 2022 Activated Neutrophils Secrete Chitinase-Like 1 and
852 Attenuate Liver Inflammation by Inhibiting Pro-Inflammatory Macrophage Responses. Front
853 Immunol **13:** 824385.
854 MALIK, P., N. CHAUDHRY, R. MITTAL AND T. K. MUKHERJEE, 2015 Role of receptor for advanced glycation end
855 products in the complication and progression of various types of cancers. Biochim Biophys Acta
856 **1850:** 1898-1904.
857 MANGIONE, F., AND E. MARTIN-BLANCO, 2018 The Dachsous/Fat/Four-Jointed Pathway Directs the Uniform
858 Axial Orientation of Epithelial Cells in the Drosophila Abdomen. Cell Rep **25:** 2836-2850 e2834.
859 MASEL, J., AND M. L. SIEGAL, 2009 Robustness: mechanisms and consequences. Trends Genet **25:** 395-403.
860 MAZUR, M., A. ZIELINSKA, M. M. GRZYBOWSKI, J. OLCZAK AND J. FICHNA, 2021 Chitinases and Chitinase-Like
861 Proteins as Therapeutic Targets in Inflammatory Diseases, with a Special Focus on Inflammatory
862 Bowel Diseases. Int J Mol Sci **22**.
863 MEISTER, M., C. HETRU AND J. A. HOFFMANN, 2000 The antimicrobial host defense of Drosophila. Curr Top
864 Microbiol Immunol **248:** 17-36.
865 MENG, G., Y. ZHAO, X. BAI, Y. LIU, T. J. GREEN *et al.*, 2010 Structure of human stabilin-1 interacting chitinase-
866 like protein (SI-CLP) reveals a saccharide-binding cleft with lower sugar-binding selectivity. J Biol
867 Chem **285:** 39898-39904.
868 MICHEL, M., AND C. DAHMANN, 2020 Tissue mechanical properties modulate cell extrusion in the
869 Drosophila abdominal epidermis. Development **147**.
870 MIRTH, C. K., AND A. W. SHINGLETON, 2012 Integrating body and organ size in Drosophila: recent advances
871 and outstanding problems. Front Endocrinol (Lausanne) **3:** 49.

MIYASHITA, K., AND T. FUJII, 1993 Nucleotide sequence and analysis of a gene (chiA) for a chitinase from Streptomyces lividans 66. Biosci Biotechnol Biochem **57:** 1691-1698.

MUSSO, G., M. COSTANZO, M. HUANGFU, A. M. SMITH, J. PAW *et al.*, 2008 The extensive and condition-dependent nature of epistasis among whole-genome duplicates in yeast. Genome Res **18:** 1092-1099.

NARDI, J. B., C. M. BEE AND C. L. WALLACE, 2018 Remodeling of the abdominal epithelial monolayer during the larva-pupa-adult transformation of Manduca. Dev Biol **438:** 10-22.

NINOV, N., D. A. CHIARELLI AND E. MARTIN-BLANCO, 2007 Extrinsic and intrinsic mechanisms directing epithelial cell sheet replacement during Drosophila metamorphosis. Development **134:** 367-379.

NINOV, N., S. MENEZES-CABRAL, C. PRAT-ROJO, C. MANJON, A. WEISS *et al.*, 2010 Dpp signaling directs cell motility and invasiveness during epithelial morphogenesis. Curr Biol **20:** 513-520.

NYIRKOS, P., AND E. E. GOLDS, 1990 Human synovial cells secrete a 39 kDa protein similar to a bovine mammary protein expressed during the non-lactating period. Biochem J **269:** 265-268.

OSTERFIELD, M., C. A. BERG AND S. Y. SHVARTSMAN, 2017 Epithelial Patterning, Morphogenesis, and Evolution: Drosophila Eggshell as a Model. Dev Cell **41:** 337-348.

OSTERFIELD, M., X. DU, T. SCHUPBACH, E. WIESCHAUS AND S. Y. SHVARTSMAN, 2013 Three-dimensional epithelial morphogenesis in the developing Drosophila egg. Dev Cell **24:** 400-410.

PANZADE, S., AND M. MATIS, 2021 The Microtubule Minus-End Binding Protein Patronin Is Required for the Epithelial Remodeling in the Drosophila Abdomen. Front Cell Dev Biol **9:** 682083.

PESCH, Y. Y., D. RIEDEL, K. R. PATIL, G. LOCH AND M. BEHR, 2016 Chitinases and Imaginal disc growth factors organize the extracellular matrix formation at barrier tissues in insects. Sci Rep **6:** 18340.

PINTEAC, R., X. MONTALBAN AND M. COMABELLA, 2021 Chitinases and chitinase-like proteins as biomarkers in neurologic disorders. Neurol Neuroimmunol Neuroinflamm **8**.

PRAT-ROJO, C., P. A. POUILLE, J. BUCETA AND E. MARTIN-BLANCO, 2020 Mechanical coordination is sufficient to promote tissue replacement during metamorphosis in Drosophila. EMBO J **39:** e103594.

QURESHI, A. M., A. HANNIGAN, D. CAMPBELL, C. NIXON AND J. B. WILSON, 2011 Chitinase-like proteins are autoantigens in a model of inflammation-promoted incipient neoplasia. Genes Cancer **2:** 74-87.

RAMESH, P., N. S. DEY, A. KANWAL, S. MANDAL AND L. MANDAL, 2021 Relish plays a dynamic role in the niche to modulate Drosophila blood progenitor homeostasis in development and infection. Elife **10**.

RECKLIES, A. D., C. WHITE AND H. LING, 2002 The chitinase 3-like protein human cartilage glycoprotein 39 (HC-gp39) stimulates proliferation of human connective-tissue cells and activates both extracellular signal-regulated kinase- and protein kinase B-mediated signalling pathways. Biochem J **365:** 119-126.

RENKEMA, G. H., R. G. BOOT, F. L. AU, W. E. DONKER-KOOPMAN, A. STRIJLAND *et al.*, 1998 Chitotriosidase, a chitinase, and the 39-kDa human cartilage glycoprotein, a chitin-binding lectin, are homologues of family 18 glycosyl hydrolases secreted by human macrophages. Eur J Biochem **251:** 504-509.

RICHARDSON, B. E., AND R. LEHMANN, 2010 Mechanisms guiding primordial germ cell migration: strategies from different organisms. Nat Rev Mol Cell Biol **11:** 37-49.

RITTENHOUSE, K. R., AND C. A. BERG, 1995 Mutations in the *Drosophila* gene *bullwinkle* cause the formation of abnormal eggshell structures and bicaudal embryos. Development **121:** 3023-3033.

ROSNER, B. A., 2000 *Fundamentals of Biostatistics*. Duxbury Press, Pacific Grove, CA.

ROSSI, A., Z. KONTARAKIS, C. GERRI, H. NOLTE, S. HOLPER *et al.*, 2015 Genetic compensation induced by deleterious mutations but not gene knockdowns. Nature **524:** 230-233.

RUDRAPATNA, V. A., E. BANGI AND R. L. CAGAN, 2014 A Jnk-Rho-Actin remodeling positive feedback network directs Src-driven invasion. Oncogene **33:** 2801-2806.

RYDER, E., F. BLOWS, M. ASHBURNER, R. BAUTISTA-LLACER, D. COULSON *et al.*, 2004 The DrosDel collection: a set of P-element insertions for generating custom chromosomal aberrations in Drosophila melanogaster. Genetics **167:** 797-813.

920 SAMAC, D. A., C. M. HIRONAKA, P. E. YALLALY AND D. M. SHAH, 1990 Isolation and Characterization of the
921 Genes Encoding Basic and Acidic Chitinase in Arabidopsis thaliana. Plant Physiol **93:** 907-914.
922 SAROV, M., C. BARZ, H. JAMBOR, M. Y. HEIN, C. SCHMIED *et al.*, 2016 A genome-wide resource for the analysis
923 of protein localisation in Drosophila. Elife **5:** e12068.
924 SCHIMPL, M., C. L. RUSH, M. BETOU, I. M. EGGLESTON, A. D. RECKLIES *et al.*, 2012 Human YKL-39 is a pseudo-
925 chitinase with retained chitooligosaccharide-binding properties. Biochem J **446:** 149-157.
926 SHAO, R., K. HAMEL, L. PETERSEN, Q. J. CAO, R. B. ARENAS *et al.*, 2009 YKL-40, a secreted glycoprotein,
927 promotes tumor angiogenesis. Oncogene **28:** 4456-4468.
928 SHARABI, K., A. HURWITZ, A. J. SIMON, G. J. BEITEL, R. I. MORIMOTO *et al.*, 2009a Elevated CO2 levels affect
929 development, motility, and fertility and extend life span in Caenorhabditis elegans. Proc Natl
930 Acad Sci U S A **106:** 4024-4029.
931 SHARABI, K., E. LECUONA, I. T. HELENIUS, G. J. BEITEL, J. I. SZNAJDER *et al.*, 2009b Sensing, physiological effects
932 and molecular response to elevated CO2 levels in eukaryotes. J Cell Mol Med **13:** 4304-4318.
933 SIOMAVA, N., E. A. WIMMER AND N. POSNIEN, 2016 Size relationships of different body parts in the three
934 dipteran species Drosophila melanogaster, Ceratitis capitata and Musca domestica. Dev Genes
935 Evol **226:** 245-256.
936 SOKAC, A. M., N. BIEL AND S. DE RENZIS, 2022 Membrane-actin interactions in morphogenesis: Lessons
937 learned from Drosophila cellularization. Semin Cell Dev Biol.
938 SUTHERLAND, T. E., N. LOGAN, D. RUCKERL, A. A. HUMBLES, S. M. ALLAN *et al.*, 2014 Chitinase-like proteins
939 promote IL-17-mediated neutrophilia in a tradeoff between nematode killing and host damage.
940 Nat Immunol **15:** 1116-1125.
941 SWARUP, S., AND E. M. VERHEYEN, 2012 Wnt/Wingless signaling in Drosophila. Cold Spring Harb Perspect
942 Biol **4**.
943 THARANATHAN, R. N., AND F. S. KITTUR, 2003 Chitin--the undisputed biomolecule of great potential. Crit Rev
944 Food Sci Nutr **43:** 61-87.
945 TORRES, E. M., B. R. WILLIAMS AND A. AMON, 2008 Aneuploidy: cells losing their balance. Genetics **179:** 737-
946 746.
947 TRAN, D. H., AND C. A. BERG, 2003 *bullwinkle* and *shark* regulate dorsal-appendage morphogenesis in
948 *Drosophila* oogenesis. Development **130:** 6273-6282.
949 TSIGKARI, K. K., S. F. ACEVEDO AND E. M. SKOULAKIS, 2012 14-3-3epsilon Is required for germ cell migration in
950 Drosophila. PLoS One **7:** e36702.
951 ULMSCHNEIDER, B., B. K. GRILLO-HILL, M. BENITEZ, D. R. AZIMOVA, D. L. BARBER *et al.*, 2016 Increased
952 intracellular pH is necessary for adult epithelial and embryonic stem cell differentiation. J Cell
953 Biol **215:** 345-355.
954 VARELA, P. F., A. S. LLERA, R. A. MARIUZZA AND J. TORMO, 2002 Crystal structure of imaginal disc growth
955 factor-2. A member of a new family of growth-promoting glycoproteins from *Drosophila*
956 *melanogaster*. J Biol Chem **277:** 13229-13236.
957 VENKEN, K. J., Y. HE, R. A. HOSKINS AND H. J. BELLEN, 2006 P[acman]: a BAC transgenic platform for targeted
958 insertion of large DNA fragments in D. melanogaster. Science **314:** 1747-1751.
959 WARD, E. J., AND C. A. BERG, 2005 Juxtaposition between two cell types is necessary for dorsal appendage
960 tube formation. Mech Dev **122:** 241-255.
961 WATANABE, T., K. KOBORI, K. MIYASHITA, T. FUJII, H. SAKAI *et al.*, 1993 Identification of glutamic acid 204 and
962 aspartic acid 200 in chitinase A1 of Bacillus circulans WL-12 as essential residues for chitinase
963 activity. J Biol Chem **268:** 18567-18572.
964 ZHANG, J., A. GRATCHEV, V. RIABOV, S. MAMIDI, C. SCHMUTTERMAIER *et al.*, 2009 A novel GGA-binding site is
965 required for intracellular sorting mediated by stabilin-1. Mol Cell Biol **29:** 6097-6105.

ZIMMERMAN, S. G., G. E. MERRIHEW, M. J. MACCOSS AND C. A. BERG, 2017 Proteomics Analysis Identifies Orthologs of Human Chitinase-Like Proteins as Inducers of Tube Morphogenesis Defects in Drosophila melanogaster. Genetics **206:** 973-984.

ZUROVCOVA, M., AND F. J. AYALA, 2002 Polymorphism patterns in two tightly linked developmental genes, Idgf1 and Idgf3, of Drosophila melanogaster. Genetics **162:** 177-188.

Supplementary Figures and Tables

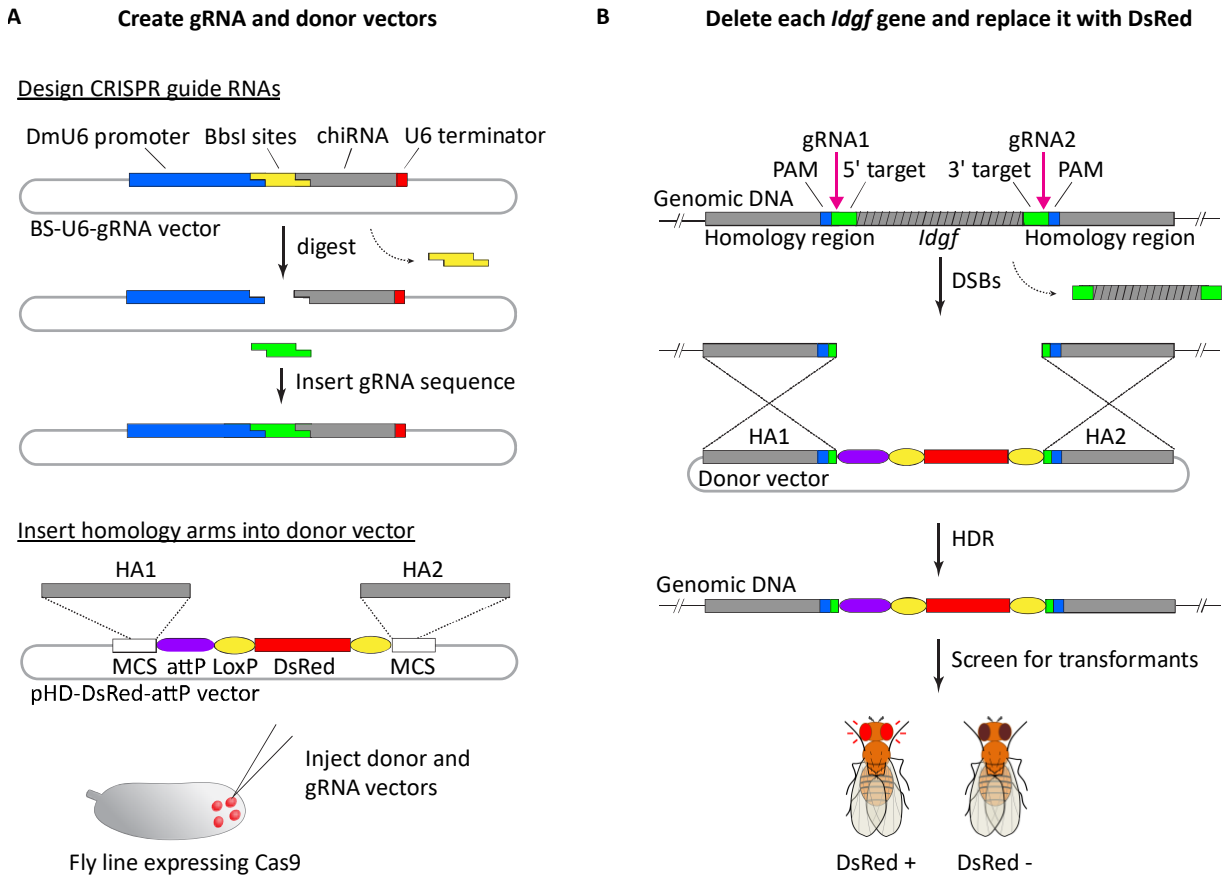

Figure S1 *Idgf* gene deletion method. (A) Strategy for constructing gRNA vectors and donor vectors for injection into embryos endogenously expressing Cas9. (B) Cas9 exploits gRNAs to make double-strand breaks at sites of pink arrows. Using homology directed repair, the *Idgf* gene is replaced with the gene encoding DsRed fluorescent protein. Transformants are null for the *Idgf* gene of interest and have fluorescent red eyes. gRNA (guide RNA), HA (homology arm), MCS (multiple cloning site) PAM (protospacer adjacent motif), DSB (double-strand break) HDR (homology directed repair).

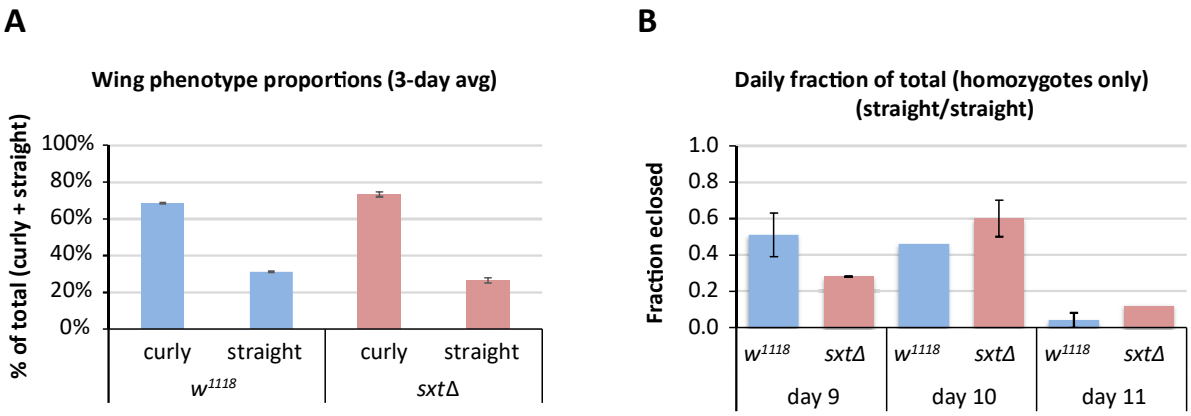

983
984 **Figure S2 Eclosion rates**. (A) Eclosion averaged over 3 days [9-11 days after egg laying (AEL)] for offspring of *+*;
985 *+/CyO* and w^{1118} $Idgf^{4\Delta}$; $Idgf^{(1-3)\Delta,(6-5)\Delta}$/*CyO* crosses. Percentages are the number of curly or straight-winged flies
986 divided by the total (curly + straight). The expected Mendelian fractions of curly vs. straight-winged flies should be
987 2/3 heterozygous (curly-winged) and 1/3 homozyous (straight-winged) flies. The relative fractions of wing
988 phenotypes in the *sxtΔ* background (73% curly, 27% straight) deviates significantly from the relative fractions in
989 the w^{1118} background (69% curly, 31% straight) (p = 0.0087, X^2 test, n=1304 for the w^{1118} background and 1185 for
990 the *sxtΔ* background). (B) Eclosion rates for homozygous offspring over time. Fractions are the number of
991 homozygous flies eclosed for each day divided by the total number of homozygous flies for all three days. The
992 fraction of w^{1118} homozygotes peaks 1 day earlier than for the *sxtΔ* homozygotes, indicating that the *sxtΔ*
993 homozygotes are developmentally delayed.
994

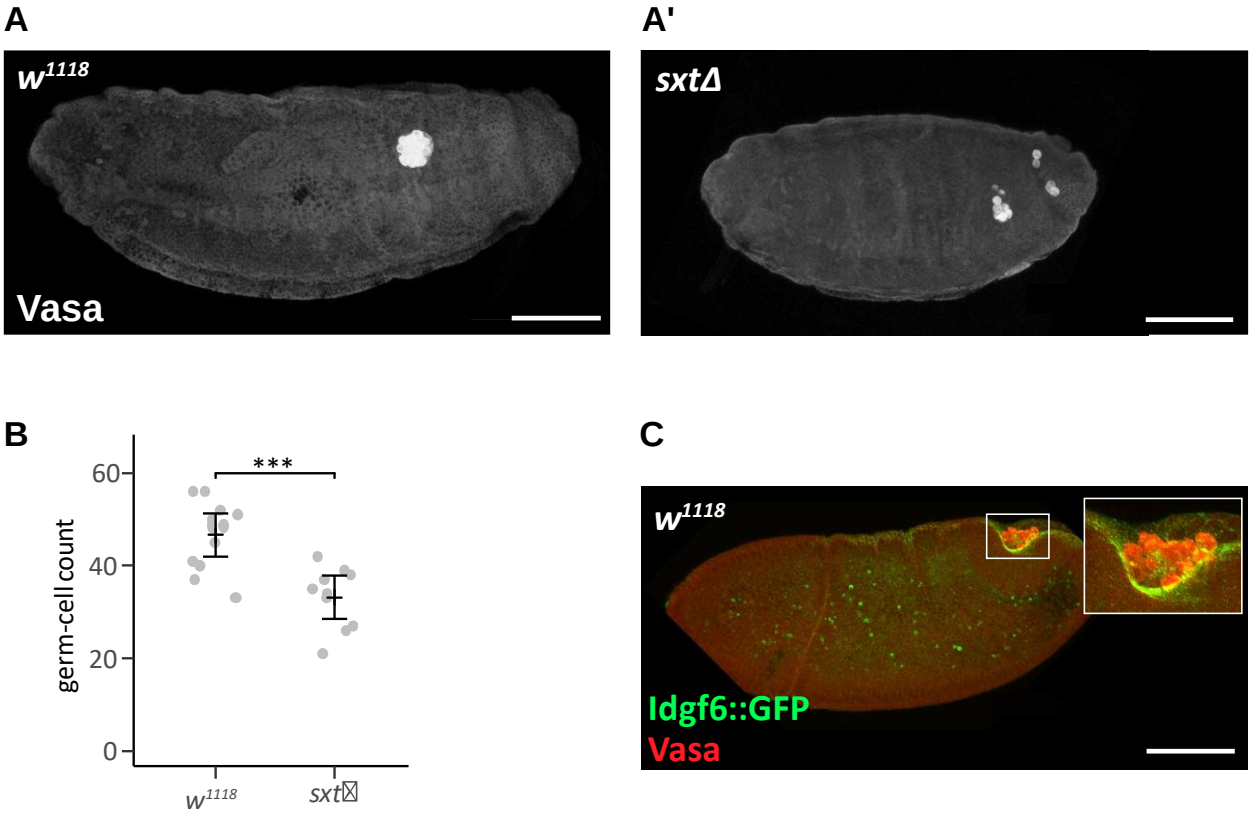

Figure S3 Germ cell migration. Anterior is to the left, dorsal is up in A, A', and C. (A, A') Germ cells in 16-hour old embryos are marked with anti-Vasa antibody, revealing germ-cell loss and reduced numbers in the gonads of sxtΔ versus w^{1118} embryos. Scale bar = 50µm. (B) Graph shows germ cell counts in individual 3-hour old cellular blastoderm embryos. w^{1118}, mean = 46.6 (n= 12 embryos), *sxtΔ*, mean = 33.2 (n= 10 embryos), $p = 0.0002$, Student's *t*-test. (C) During germband extension, GFP-tagged Idgf6 (green) is present in and around the pole cells, which are marked with anti-Vasa antibody (red). Scale bars = 100µm.

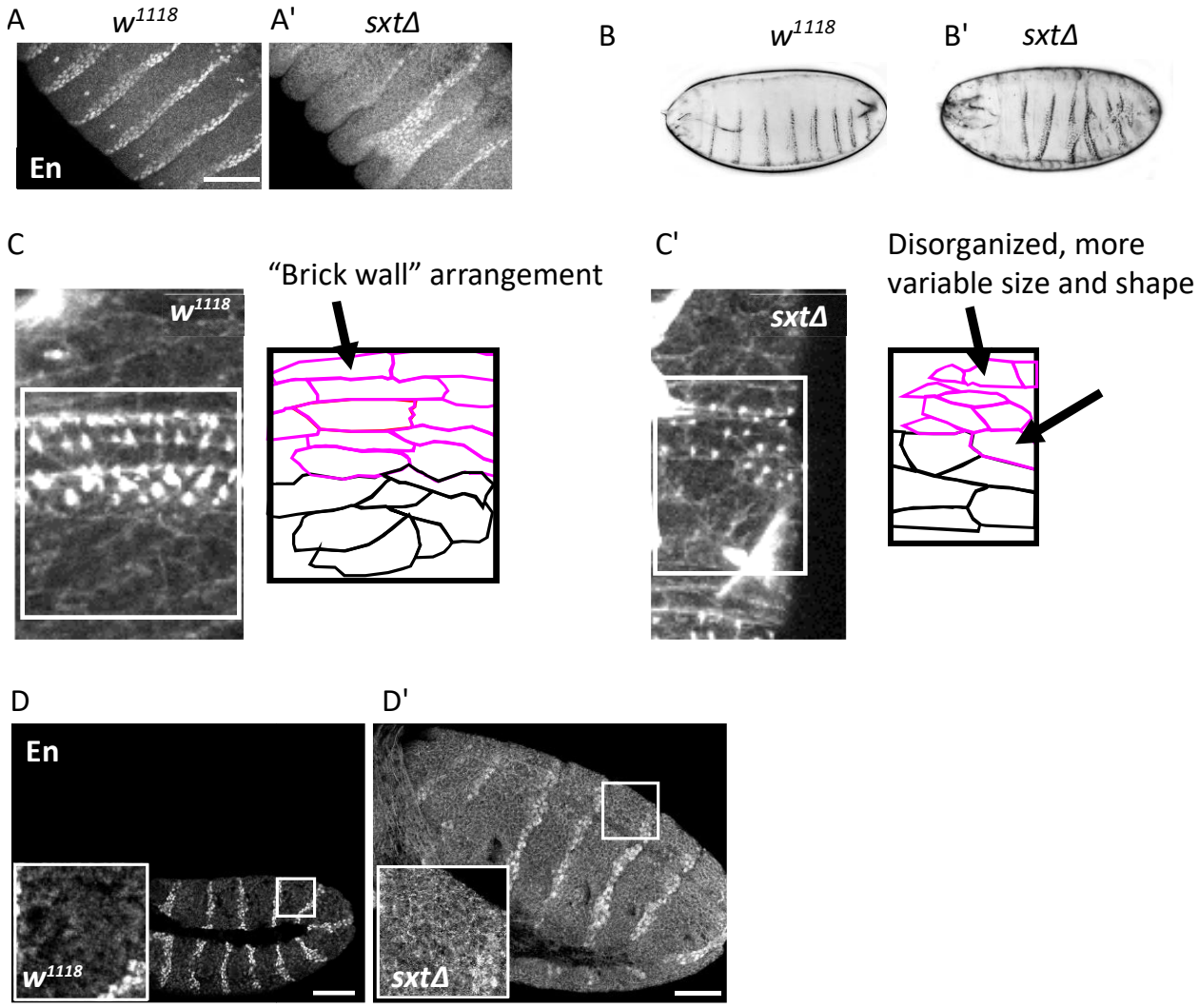

Figure S4 Segmentation defects. (A,A') Anti-Engrailed antibody marks the posterior cells in each segment in w^{1118} embryos. *sxtΔ* mutants exhibit segmentation defects. Scale bar = 50µm. (B,B') Denticle belt defects in *sxtΔ* mutants reflect segmentation defects. Lateral view (B), ventrolateral view (B'). (C,C') In Stage 16 embryos, Rhodamine-Phalloidin highlights cell cortices and the actin protrusions that secrete cuticle to form denticles (images). White squares in images show the areas drawn in the diagrams. (C) The control (w^{1118}) cells display the typical "brick wall" arrangement in the denticle-producing cells (magenta) and the larger, less organized naked cuticle cells (black). (C') Cell morphology and localization in denticle-producing cells is disrupted in *sxtΔ* mutant embryos. (D,D') Engrailed protein aberrantly localizes to cell membranes in *sxtΔ* embryos (C'), but not in w^{1118} embryos (C). White rectangle indicates area shown in close-up. Scale bar = 50µm.

1017

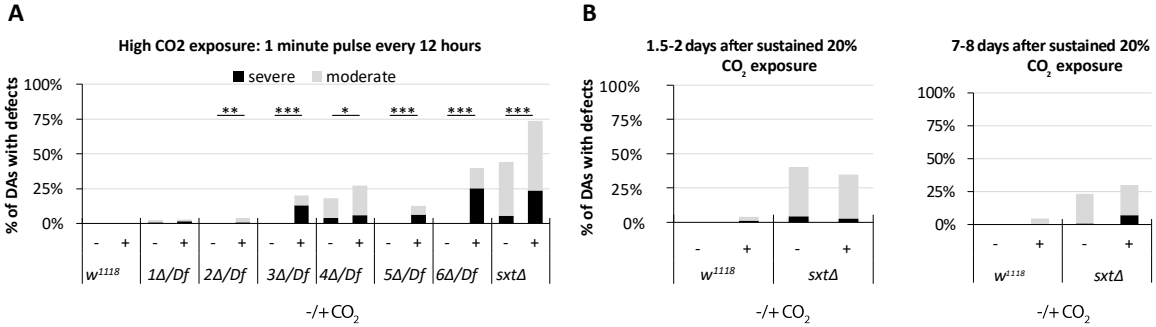

1018

1019 **Figure S5 CO_2 Exposure regimes.** DA defects are significantly increased in *Idgf2Δ*, *Idgf3Δ, Idgf4Δ*, *Idgf5Δ*, *Idgf6Δ*,
1020 and *sxtΔ* mutants after a one-minute pulse of high (100%) CO_2 exposure every 12 hours. A sustained time course
1021 of 20% CO2 for at least 1.5 days and as much as 8 days does not significantly increase DA defects in these mutants.
1022 * denotes $p<0.05$, ** denotes $p<0.01$, *** denotes $p<0.001$, Bonferroni adjusted p-values, X^2 test for trends in
1023 binomial proportions (ROSNER 2000).
1024

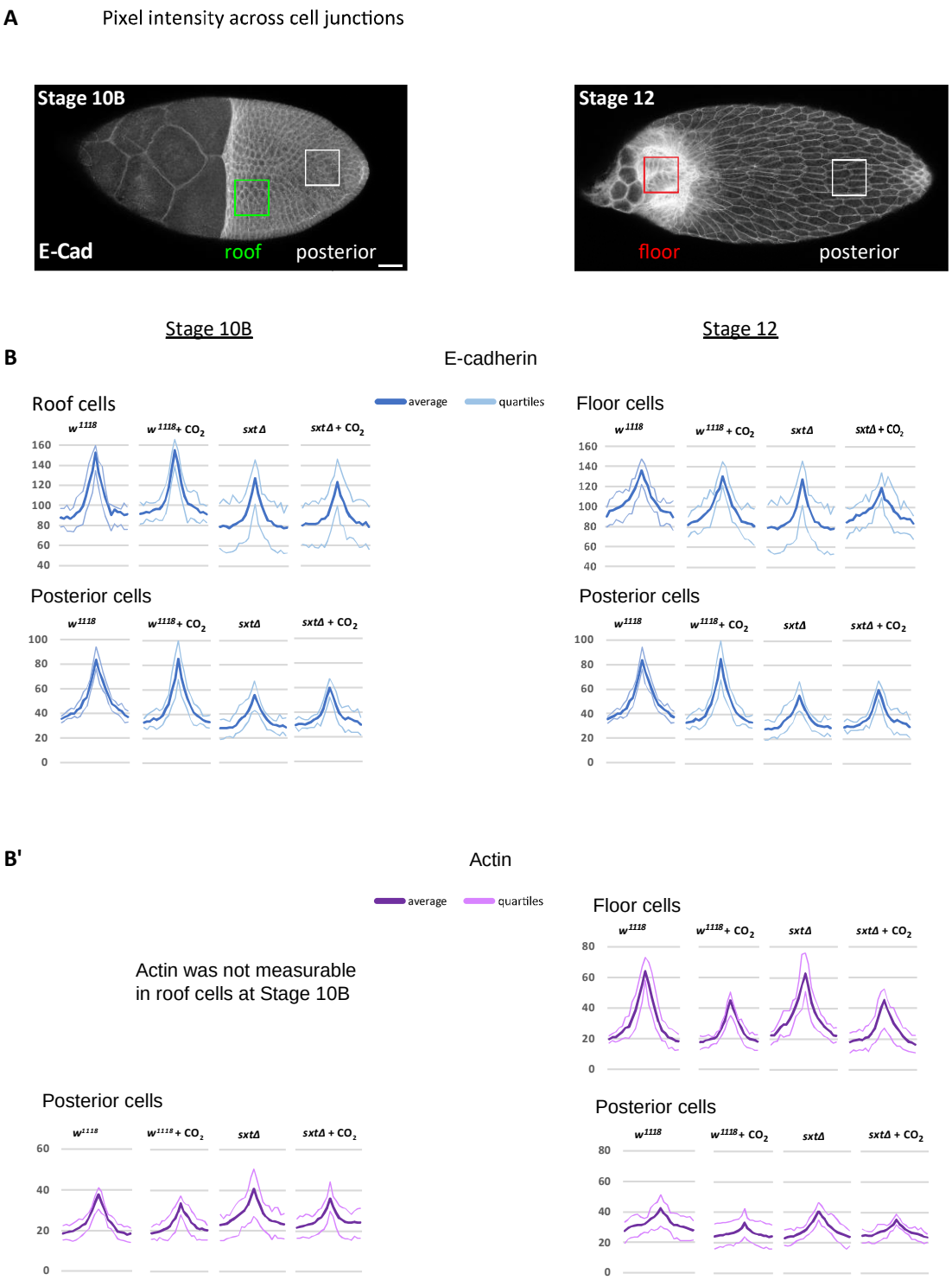

Figure S6 Quantification of cortical Actin and E-Cadherin intensity in DA cells. (A) E-Cadherin and Actin in Stage 10B roof cells (green square) and Stage 12 floor cells (red square) and in posterior columnar cells (white squares). (B) Comparison of w^{1118} and *sxtΔ* fluorescence intensity plot profiles averaged across three cell membranes, from the center of one cell to the center of the neighboring cell, averaged over at least 6 egg chambers for each genotype and each exposure regime as indicated. Plots show mean (E-cad, blue and Actin, magenta) and confidence limits (gray).

1032 **Table S1 Molecularly mapped *Idgf* gene loci, mRNA, protein lengths and weights, and deleted sequences**

Gene	Locus[a]	Length (bp)	Isoform	mRNA Length (nt)	Protein Length (aa)	MW (kDa)	Deleted Sequence[b]
Idgf1	16,445,278	1516	A	1445	439	49.4	16,445,132 - 16,446,690
Idgf2	16,447,330	3179	A	1440	440	49.2	16,449,257 - 16,450,348
			B	1796	368	41.1	
			C	1367	368	41.1	
Idgf3	16,450,907	4288	A	1649	441	49.3	16,450,962 - 16,452,978
			B	3145	441	49.3	
			C	1724	441	49.3	
			D	3801	441	49.3	
Idgf4	9,927,973	2976	A	1514	442	48.6	9,928,084 - 9,930,904
			B	1541	442	48.6	
			C	1807	442	48.6	
Idgf5	18,393,666	1617	A	1495	444	50.1	18,393,347 - 18,395,294
Idgf6	16,691,022	2730	A	1541	452	50.4	16,690,912 - 16,693,893
			B	1811	452	50.4	

1033 a. 5' nucleotide locus of molecularly mapped sequence from flybase.org
1034 b. Cas9 cuts directly before the first and after the second number
1035

1036 **Table S2 Cytological locations, gRNA sequences, and cut sites. Vertical line (|) indicates gRNA cut site,**
1037 **underlined nucleotides indicate PAM (located 3' to target on genomic DNA, not part of gRNA)**

Deletion[a,f]	Cytological Location	5' gRNA Target	3' gRNA Target
Single			
Idgf$^{1\Delta}$	2L: 36A	gtgaaactgtattagct | gac agg	tacttaattgaccgcag | tat ggg
Idgf$^{2\Delta}$	2L: 36A	acttggtctacggctat | gct ggg	gccccctaggttcttga | cac ggg
Idgf$^{3\Delta}$	2L: 36A	ggggttttcgtttcact | acg ggg	gaggccttttaggcacc | gaa agg
Idgf$^{4\Delta}$	X: 9A	aaactatataaattatc | aca cgg	gacgatagtaaacttta | taa agg
Idgf$^{5\Delta}$	2R: 55C	tccacacatttgccaca | aac tgg	atagtaaacgagctttc | aaa tgg
Idgf$^{6\Delta}$	2R: 53D	ggtcacacatgctgatt | ttc agg	ggtattcaattaaattg | cgt agg
Double			
Idgf$^{2\Delta,3\Delta}$	2L: 36A	acttggtctacggctat | gct ggg	gaggccttttaggcacc | gaa agg
Idgf$^{6\Delta,5\Delta}$	2R: 53D, 55C	b	b
Triple			
Idgf$^{1\Delta,2\Delta,3\Delta}$	2L: 36A	c	c
Idgf$^{4\Delta}$;*Idgf*$^{6\Delta,5\Delta}$	X: 9A; 2R: 53D, 55C	d	d
Sextuple			
Idgf$^{4\Delta}$;Idgf$^{(1,2,3)\Delta,(6,5)\Delta}$	X: 9A; 2L: 36A; 2R: 53D, 55C	e	e

1038 a. Additional null combinations may be generated by crossing or recombining the applicable null lines.
1039 b. Generated by recombination between *Idgf6*Δ and *Idgf5*Δ
1040 c. *Idgf1* guide and donor plasmids were injected into *vas-Cas9GFP*; *Idgf2Δ3*Δ embryos to preserve integrity of the
1041 neighboring gene *CG5888*
1042 d. Generated by crossing *Idgf*$^{6\Delta,5\Delta}$ to *Idgf*$^{4\Delta}$
1043 e. Generated by recombination between *Idgf*$^{1\Delta,2\Delta,3\Delta}$ and *Idgf*$^{6\Delta,5\Delta}$ followed by cross to *Idgf*$^{4\Delta}$ line
1044 f. All the lines are in a *w*^{1118} background

1045

1046 **Table S3 Deficiency phenotypes. The deficiencies delete the indicated Idgfs. Deficiency locus is heterozygous**
1047 **with wild-type Idgf(s) to test for DA defects caused by deletion of genes flanking the Idgfs within the**
1048 **deletion locus.**

genotype	associated Idgf deletions	normal	moderate	severe
w^{1118}; +/+	NA	98.4%	1.5%	0.1%
w^{1118}; +/Df(2L)ED1102 (VENKEN *et al.* 2006)*; +*	1Δ, 2Δ, 3Δ	99.1%	0.7%	0.1%
w^{1118}/Df(1)ED6989 (VENKEN *et al.* 2006)	4Δ	100.0%	0.0%	0.0%
w^{1118}; +/Df(2R)BSC337; +	5Δ	99.8%	0.2%	0.0%
w^{1118}; +/Df(2R)6064; +	6Δ	99.4%	2.0%	0.0%

1049